REPORT DOCUMENTATION PAGE

Form Approved
OMB No. 074-0188

1. AGENCY USE ONLY (Leave blank)	2. REPORT DATE	3. REPORT TYPE AND DATES COVERED
	June 16, 2005	Final Technical (05/1/03-12/31/04)

4. TITLE AND SUBTITLE
Block Copolymer Composites: A Bio-Optic Synthetic System for Dynamic Control

5. FUNDING NUMBERS
MDA972-02-C-0-052

6. AUTHOR(S)
Gary Wnek, Ph.D.
Thomas Smith, Ph.D.

7. PERFORMING ORGANIZATION NAME(S) AND ADDRESS(ES)
Virginia Commonwealth University
School of Engineering
PO Box 843068
Richmond, VA 23284-3068

8. PERFORMING ORGANIZATION REPORT NUMBER
Final Technical for #528865

9. SPONSORING / MONITORING AGENCY NAME(S) AND ADDRESS(ES)
DARPA/DSO
Attn: Leonard Buckley
3701 North Fairfax Dr
Arlington, VA 22203-1714

10. SPONSORING / MONITORING AGENCY REPORT NUMBER

11. SUPPLEMENTARY NOTES

12a. DISTRIBUTION / AVAILABILITY STATEMENT
APPROVED FOR PUBLIC RELEASE; distribution is Unlimited

12b. DISTRIBUTION CODE

13. ABSTRACT *(Maximum 200 Words)*

This 18 month program focused on the development of hybrid polymer systems capable of dynamic refractive index change using electric field modulation.

14. SUBJECT TERMS
hybrid polymer systems

15. NUMBER OF PAGES
8

16. PRICE CODE

17. SECURITY CLASSIFICATION OF REPORT	18. SECURITY CLASSIFICATION OF THIS PAGE	19. SECURITY CLASSIFICATION OF ABSTRACT	20. LIMITATION OF ABSTRACT
Unclassified	Unclassified	Unclassified	SAR

NSN 7540-01-280-5500

Standard Form 298 (Rev. 2-89)
Prescribed by ANSI Std. Z39-18
298-102

Block Copolymer Composites: A Bio-Optic Synthetic System for Dynamic Control of Refractive Index

Gary E. Wnek*
Virginia Commonwealth University

and

Thomas W. Smith
Rochester Institute of Technology

This material is based upon work supported by the Defense Advanced Research Projects Agency Defense Sciences Office DARPA Order No N540/00 Program Code: 2Y10 Issued by DARPA/CMO under Contract #MDA972-02-C-0052

---

* Current affiliation – Case Western Reserve University

Block copolymer Composites: A Bio-Optic Synthetic System for Dynamic Control of Refractive Index.

Task Objectives

This 18-month program focused on the development of hybrid polymer systems capable of dynamic refractive index change ($\Delta\eta$of at least 0.5) using electric field modulation.

Technical Problems

There are materials (liquid crystals, $LiNbO_3$, KH_2PO_4, etc.) whose refractive index can be modulated by application of an electric field; the change in refractive index, however, is typically small, $\Delta\eta \leq .05$. Moreover, with the exception of polymer dispersed liquid crystals, options for engineering these materials in the fabrication of lenses or microlens arrays are limited.

General methodology

In the quest for systems capable of dynamic refractive index change,$\Delta\eta$,of at least 0.5, we proposed three new materials-based options. The first, depicted in Figure 1, is the spatial modulation of refractive index by Maxwell-Wagner (interfacial) polarization of dispersed, ion-conductive phases in PS-b-PEO containing NLO-active moieties. In this initiative we postulate that change of refractive index will result from the electric field induced orientation and polarization of NLO-active moieties or nanocrystals sequestered in the PEO domains of the block compolymer.

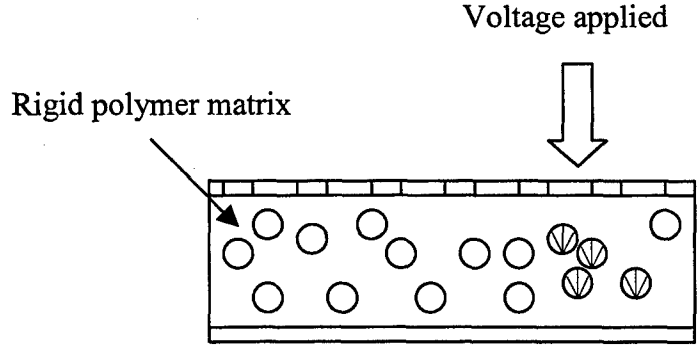

Electric field induced orientation and polarization of dispersed domains.

Figure 1

The second is the image-wise deformation and shape change of an elastomeric composite *a'la* the γ-Ruticon. In this approach we envisioned a deformation light valve wherein the thickness of a lightly crosslinked PDMS-g-PEO/salt composite is modulated in accordance with the frequency of an interdigitated comb electrode.

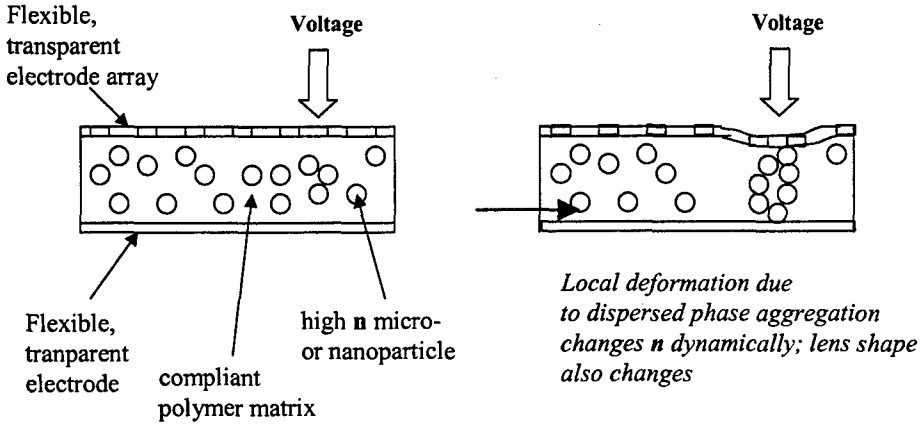

Figure 2

The last approach is a microlens whose shape is changed by electrocapillary effects in gels or fluids by application of an electric field. An example of this approach is shown in Figure 3.

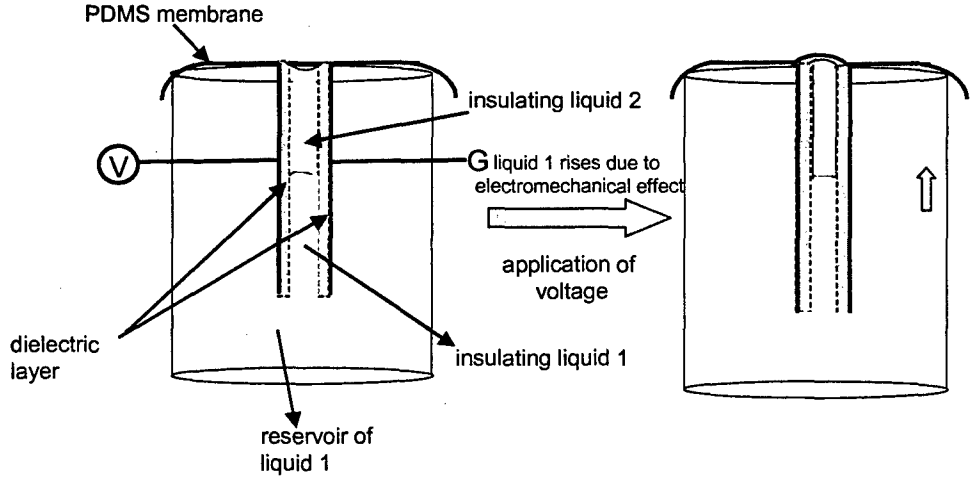

Figure 3

Here we envisioned the use of two immiscible colorless insulating liquids where in the shape of the meniscus of liquid 2 (in the figure 3) can be adjusted by application of a voltage thereby controlling the focal length. Additionally in principle, this methodology should allow us further control of the focal length by adjusting the meniscus shape at the interface of liquids 1 and 2. This can be achieved by an appropriate choice of the liquids (hydrophobic/hydrophilic).

Finally we also envisioned formation of transparent mats using electrostatic processing by carefully adjusting fiber alignment. The final goal is to encapsulate appropriate materials within these aligned fibers so as to manipulate refractive index of the overall electrospun mat either by application of an electric or magnetic field.

Technical Results

Spatial modulation of refractive index in PS-b-PEO composites.

Over the 18 month horizon of the grant, we doped ionophoric and ionomeric block copolymers containing poly(ethylene oxide), PEO, and poly(acrylic acid), PAA, chain segments with ionizable salts and polarizable, electrorefractive moieties and nanocrystals. Simple devices comprised of thin films of PS-b-PEO/KDP, PS-b-PEO/2-amino-5-nitropyridinium salts and PS-b-PEO/$CdCl_2$/4-nitropyridine N-oxide composites spin-coated onto transparent ITO-coated glass substrates and surface-coated with transparent gold electrodes were fabricated.

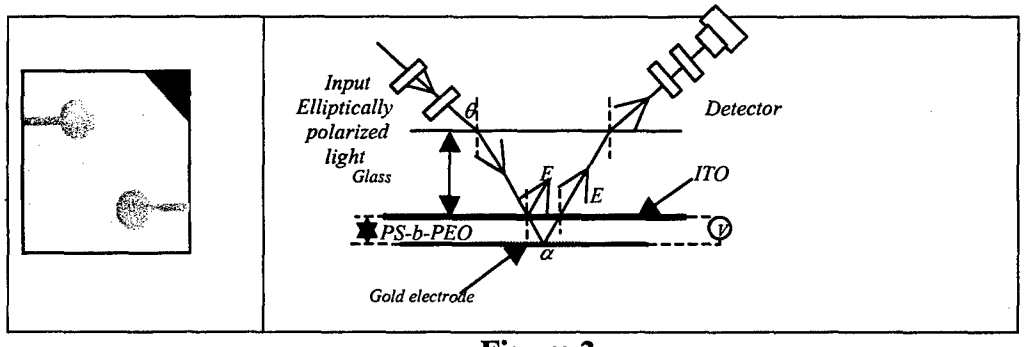

Figure 3

Figure 3 shows a diagram of the optical configuration of the experimental setup adapted from that taught by Teng and Man (Appl. Phys. Lett., Vol. 56, No. 18, 1990) for ellipsometric evaluation of electro-optic characteristics of materials. Elliptically polarized light is reflected off the back of the glass substrate (off the semitransparent gold layer) at an angle, θ, and propagates through the substrate, the ITO, the polymer layer and back into the air where it is collected. When a modulating voltage is applied across the electrodes, a change in the ellipticity is induced by the change in refractive index. There is also a change in the path length due to the change in the reflections angle accompanying the change in refractive index.

In our work, a thin film of polymer of the order of a few microns (3-6 μm) was spin coated on an ITO-coated glass substrate. The ITO served as one of two electrodes used to apply a poling field. The second electrodes is a semitransparent (~200 Å) gold film that was evaporated in two ~15 mm circular areas on the surface of the film. These electrodes allowed us to modulate the field in the electro-optic measurement. With two circularly patterned electrodes, we attempted to evaluate electro-optic characteristics of the same sample in poled and un-poled states. A manual ellipsometer in the laboratories at RIT was used to qualitatively examined thin films of PS-b-PEO/KDP, PS-b-PEO/2-amino-5-nitropyridinium salts and PS-b-PEO/$CdCl_2$/4-nitropyridine N-oxide composites for electrooptic activity by observation of deviation of the meter from null. While some films of PS-b-PEO/2-amino-5-nitropyridinium dihydrogen phosphate composites appeared to shown an electrorefractive response, apparent problems relative to instability

of PS-b-PEO/2-amino-5-nitropyridinium dihydrogen phosphate composites and delamination of the gold electrodes after application of electric field frustrated efforts to validate and quantify any electrorefractive response.

DSC characteristics of PS-b-PEO complexes were also evaluated. While results indicated significant complexity in the nature of the composites formed in PS-b-PEO, an endotherm indicative of a crystalline material melting at about 250°C was consistently observed in DSC scans on transparent (non-scattering) annealed films cast from solutions of PS-b-PEO doped with H_3PO_4 and neutralized with one equivalent of KOH. We have interpreted these results as being evidentiary of the presence of KH_2PO_4 nanocrystals in doped PS-b-PEO films.

Image-wise deformation of an elastomeric composite.
Deformation an elastomeric composite *comprised of* crosslinked graft copolymer of poly(dimethylsiloxane) and oligo-ethylene oxide doped with salt was demonstrated. Films of the elastomer were coated onto glass substrates bearing a pattern of interdigitated gold electrodes and metallized with thin semitransparent gold layers that serves as both a mirror and a counter-electrode. Application of a to the interdigitated electrode array produce a deformation pattern. In our crosslinked graft copolymer of poly(dimethylsiloxane) and oligo-ethylene oxide, doped with salt, the attractive potential between the polarized PEO salt domains is the driving force for deformation and localized change in refractive index that will result from positional dislocation. The magnitude of the deformation realized was only of the order of the thickness of the semitransparent gold layer, 20-50nm, and was not sufficient magnitude to provide a change in refractive index required by the project. .

Electrocapillarity.
The choice of the two immiscible liquids is an important parameter in order to achieve any sort of control over the initial meniscus. In general a long chain (nonvolatile) hydrocarbon or fluorocarbon and a polar nonvolatile liquids can be employed as liquid 2 and liquid 1 respectively. Using this we were able to manipulate the shape of the liquid meniscus. However problems of breakdown within the capillary did not allow us sufficient control. We believe employing a dielectric coating (such as Parylene or silicon nitride) inside the capillary can prevent this. We have also demonstrated the basic concept of this device by simply using mechanical means (such as pressure). Thus, a combination of electrical and mechanical forces (electromechanical) may be more effective. Finally the refractive index of the liquids can be controlled in principle by suspending nanoparticles in the liquids, which are sensitive to application of electric field.

Transparent Mats using Electrostatic Processing.
This methodology has two issued which have to be carefully considered; ensuring that fibers are obtained (as opposed to beads or beaded fibers) and secondly alignment of these fibers. In electrospinning, the presence of residual charge on the fibers leads to bending instabilities, which produces a whipping like motion and formation of nonwoven opaque mats. Firstly, we have developed a straightforward approach to predict the transition from beads to beaded fibers and finally fibers using parameters from polymer

solution rheology. Finally we were able to fabricate aligned mats by controlling the applied voltage. Interestingly, using this methodology we were able to obtain aligned mats with copper particle. The relevant papers are attached to this document. In the final step we plan to develop aligned mats encapsulating relevant materials to control refractive index.

Findings and Conclusions

- With the completion of this effort to development of hybrid polymer systems capable of dynamic refractive index change ($\Delta\eta$of at least 0.5) using electric field modulation we have been not been able to demonstrate that an electrorefractive response can be realized by the spatial modulation of refractive index by Maxwell-Wagner (interfacial) polarization of dispersed, ion-conductive phases in PS-b-PEO containing NLO-active moieties.
- We were able to observe *image-wise deformation of thin films of an elastomeric composite* comprised of lightly crosslinked PDMS-graft-PEO doped with salt. However, the magnitude of the deformation was insufficient to realize the goals of the project.

Implications for Further Research

As a spin off of the funding from DARPA/CMO Contract #MDA972-02-C-0052, work is ongoing at RIT on the preparation and characterization of ordered nanocrystalline composites of KH_2PO_4 in PS-b-PEO matrices. This work will be embodied in the M.S. thesis of RIT Chemistry graduate student, Mufadal Ayubali who is working to optimize conditions for formation of PS-b-PEO composites containing nanocrystals of KDP ADP and the like and to visualize these nanocrystals with atomic force microscopy. The work has also stimulated the thesis proposal, *"Electro-optic Adaptive Microlens,"* of RIT Microsystems Engineering Ph.D. candidate, Dale Ewbank.

Standard Form 298, Report documentation page

Publications and invited presentation in which portions of this research has been disclosed include:

Mufadal Ayubali,; Michael Kotlarchyk,; Andreas Langner and Thomas W. Smith,. *"Phosphoric acid induced assembly of styrene-ethylene oxide block copolymer micelles,"* Abstracts of Papers, 229th ACS National Meeting, San Diego, CA, March 13-17, 2005 (2005), COLL-446.

Thomas W. Smith, *"Synthesis of KDP Nanocrystals in Block Copolymers of Polystyrene and Poly(oxyethylene),"* Abstracts, 32nd Northeast Regional Meeting of the American Chemical Society, Rochester, NY, October 31-November 3 (2004), GEN-049.

Thomas W. Smith and Gary E. Wnek, *"Modulation of refractive index in polymer composites: toward a synthetic bio-optic lens,"* Proceedings of SPIE-The International Society for Optical Engineering (2003), 5051[Electroactive Polymer Actuators and Devices (EAPAD)], 389-399.

S.L. Shenoy, H. L. Frisch, W. D. Bates and G. E. Wnek, "Role of Chain Entanglements on Fiber Formation During Electrospinning of Polymer Solutions: Good Solvent, Non-Specific Polymer-Polymer Interaction Limit," *Polymer*, **46**, 3372 (2005).

S. L Shenoy, W. D. Bates and G. E. Wnek, "Correlation Between "Electrospinnability" and Physical Gelation," *Polymer*, submitted (April 2005).

S. L Shenoy, W. D. Bates and G. E. Wnek, "Fabrication of Aligned Electrospun Mats by Suppression of Bending Instability," submitted to *Polymer* (June 2005).

PDF files of the published and submitted papers and abstracts of the meeting presentations are attached.

Available online at www.sciencedirect.com
SCIENCE DIRECT
Polymer 46 (2005) 3372–3384
polymer
www.elsevier.com/locate/polymer

Role of chain entanglements on fiber formation during electrospinning of polymer solutions: good solvent, non-specific polymer–polymer interaction limit

Suresh L. Shenoy[a,*], W. Douglas Bates[a], Harry L. Frisch[b], Gary E. Wnek[a,*,1]

[a]*Chemical and Life Sciences Engineering, Virginia Commonwealth University, 601 West Main Street, P.O. Box 843028, Richmond, VA 23284-3028, USA*
[b]*Department of Chemistry, University at Albany, Albany, NY 12222, USA*

Received 15 December 2004; received in revised form 3 March 2005; accepted 4 March 2005
Available online 25 March 2005

Abstract

Chain entanglements are one of many parameters that can significantly influence fiber formation during polymer electrospinning. While the importance of chain entanglements has been acknowledged, there is no clear understanding of how many entanglements are required to affect/stabilize fiber formation. In this paper, polymer solution rheology arguments have been extrapolated to formulate a semi-empirical analysis to explain the transition from electrospraying to electrospinning in the good solvent, non-specific polymer–polymer interaction limit. Utilizing entanglement and weight average molecular weights (M_e, M_w), the requisite polymer concentration for fiber formation may be determined a priori, eliminating the laborious trial-and-error methodology typically employed to produce electrospun fibers. Incipient, incomplete fiber formation is correctly predicted for a variety of polymer/solvent systems at one entanglement per chain. Complete, stable fiber formation occurs at ≥ 2.5 entanglements per chain.

Keywords: Electrospinning; Chain entanglements; Fiber formation

1. Introduction

Electrostatic spinning (electrospinning) has received a great deal of attention in the literature, especially after Reneker and co-workers [1–3] renewed interest in this phenomenon. Since then, numerous polymers have been electrospun to make fibers [4], and a comprehensive list of these spun fibers has been compiled in a recent review [5]. The ability to make ultrafine electrospun fibers makes it attractive for applications such as wound dressings [6], filtration [7,8], drug delivery [9], protective clothing for the military [10,11] and tissue scaffolds [12–14].

During the electrospinning process, under the application of an electric field a drop of polymer solution is presented at the spinneret tip. As the intensity of the electric field is increased, mutual charge repulsion on the drop surface increases, dramatically altering the droplet shape to form a Taylor cone [15]. Eventually, charge repulsion exceeds surface tension and a jet of solution is ejected from the Taylor cone towards the grounded target substrate. During jet acceleration towards the substrate, substantial solvent evaporation leaves behind polymer fibers in the form of non-woven mats. Frequently, the jet undergoes a whipping process during acceleration, which stretches the fiber and significantly reduces fiber diameter [16,17]. This allows fabrication of nanofibers even though needle diameters may be on the order of 0.5 mm.

Though the electrospinning set-up is fairly straightforward, for widespread commercial viability many important questions need to be resolved including: (a) what parameters control the fabrication of fibers as opposed to beads (as in the case of electrospraying)? (b) can fibers of uniform diameter be consistently obtained? (c) can the process be readily scaled up? (d) what are the mechanical properties of these fibers or fiber mats in comparison to bulk polymer? (e) how does the orientation of the fibers compare to

* Corresponding authors. Tel.: +1 804 440 6714; fax: +1 804 828 3846.
E-mail addresses: sshenoy@vcu.edu (S.L. Shenoy), gew5@case.edu (G.E. Wnek).
[1] Present address: Department of Chemical Engineering, Case Western Reserve University, Cleveland, OH 44106-7217, USA.

0032-3861/$ - see front matter © 2005 Elsevier Ltd. All rights reserved.
doi:10.1016/j.polymer.2005.03.011

conventional fibers? and (f) what parameters influence fiber surface morphology? Based on empirical evidence, the many parameters which affect and/or control the process of electrospinning and subsequent fiber morphology are known to be: (1) solution concentration, (2) polymer molecular weight, (3) solution viscosity, (4) solution conductivity, (5) solution surface tension, (6) applied voltage, (7) distance of source electrode from the target substrate, (8) electric field, (9) solution flow rate, (10) temperature, (11) humidity and (12) solvent volatility (see for example Ref. [18]). However, not all the variables mentioned above are fundamental control parameters nor are they independent of each other. For example, solution viscosity is a function of both concentration and polymer molecular weight (among other factors) [19]. In addition, applied voltage, target distance and electric field are all interrelated, as are target distance and solvent volatility.

Several groups have attempted to model the electrospinning process with varying amounts of success [16,17,20–29]. In these models, the electrospinning process is described as an electrohydrodynamics problem, and attempts are focused on modeling the fiber diameter as a function of the distance from the spinneret tip (or more precisely the tip of the Taylor cone). In general, these studies assume a spinnable fluid and are attempting to predict the jet diameter and bending instability process, which is responsible for generating nanoscale fibers. From a fundamental perspective, electrospun fiber diameters and morphologies are a function of solution properties (polymer concentration and molecular weight) and dynamic parameters (solvent volatility, elongational viscosity, jet velocity and flow rate) [29,30]. Utilizing the dynamic approaches above has resulted in accurate modeling of the jet instability and diameter (in particular, see Refs. [17,26, 27]). However, predicting the onset of fiber formation has not been examined to our knowledge. Frequently, the necessary conditions or a 'how-to' recipe for electrospinning a particular system is presented in an empirical fashion. We believe that concepts developed for conventional fiber spinning represent valuable background for a discussion of electrospinning, and briefly turn our attention to conventional spinning.

Among the various fiber spinning processes, electrospinning is comparable to conventional dry spinning since both processes involve polymer solutions and the removal of solvent in a gaseous environment. Arguments can be made for flash spinning to be even more relevant [31,32]; unfortunately, there is insufficient background/theoretical work on this process to make a full comparison at this time. In general, for conventional fiber spinning, 'spinnability' of the polymer solution (or melt) refers to the regime in which continuous uniform filaments are obtained [33]. In particular, instability of the extrudate during traditional fiber spinning arises from two effects: (i) capillary wave breakup (Rayleigh instability) and (ii) breakage of the fiber due to the stresses overcoming some limiting tensile strength (cohesive, brittle fracture). The spinnable regime would then occur when there are sufficient forces holding the jet together to overcome the capillary instability (lower spinnability limit). On the other hand, sufficient relaxation time (or low enough strain rates) is necessary for the material to behave in a viscoelastic manner and avoid fracture (upper spinnability limit). Note that fiber breakage due to fracture is less problematic in solution spinning in comparison to melt spinning. Nevertheless, there is an optimum range of the stabilizing forces, between which the jet is prevented from breaking into droplets (Rayleigh instability) while avoiding fracture. Although electrospinning does differ from dry-spinning in some significant ways (e.g. higher strain rates, 'whipping' draws fibers not tension, ambient temperatures, no die-swell and much thinner fibers), the fundamental instabilities that lead to formation of beaded fibers and/or fiber breakage are the same. From this perspective, electrospinning is a special case of dry spinning.

Assuming the above comparison to be valid, examining the work done on dry spinning models is then a useful exercise. Recently, Gou and McHugh [34,35] performed modeling studies on dry spun cellulose acetate (CA) from acetone. A fundamental assumption for modeling was the presence of an elastically deformable entanglement network above a critical polymer concentration or molecular weight. Their results clearly demonstrated the importance of viscoelasticity for fiber formation. The primary events in the formation of fibers by this process appear to be rapid mass transfer of the solvent and the formation of a 'skin' on the fiber. Although the electrospinning process differs from dry-spinning, these fundamental events, namely a deformable elastic model, rapid mass transfer and skin formation on the fiber surface, are expected to be similar.

Experimental observations in electrospinning confirm that for fiber formation to occur, a minimum polymer concentration is required. Below this critical value, application of voltage results in electrospraying or bead formation primarily due to a Rayleigh instability. At these low concentrations, an insufficiently deformable entangled network of polymer chains exists as discussed for conventional solution spinning above. As the polymer concentration is increased, a mixture of beads and fibers is obtained. Further increase in concentration results in formation of continuous fibers, and although it is not typically reported, at even higher polymer concentrations uniform fibers are no longer produced due to the high solution viscosity. Recently, Gupta et al. [36] and Jun et al. [37] have investigated the effect of molecular weight on continuous fiber formation at a given polymer concentration. Increased chain entanglements and longer relaxation times, a consequence of increased polymer concentration, were thought to be responsible for fiber formation. Previous publications from our laboratory have also stressed the importance of chain entanglements in electrospinning [38]. While the relevance of entanglements is generally accepted,

an analysis of their effect on the resulting morphology has not been reported.

In this regard, the results of Stephens et al. [39] are extremely valuable when discussing the utility of extrapolating solution properties to the onset of fibers. The authors employed real time Raman spectroscopy on an ejected jet to determine the polymer/solvent ratio as a function of distance from the nozzle. They concluded that at approximately 1 cm from the nozzle tip, the polymer/solvent ratio of the ejected jet remains essentially unaltered from the initial ratio in the syringe (note: their system employed tetrahydrofuran, THF, a volatile solvent). Consequently, the polymer concentration that is stabilizing the jet from capillary break-up is not changed much from the solution in the syringe barrel. Presumably, further away from the tip as the solvent evaporates, a considerable increase in polymer concentration, entanglements and elongational viscosity occurs, thereby affecting the viscoelastic properties. These results suggest that solution properties such as polymer concentration and molecular weight significantly affect fiber/bead formation in comparison to other governing parameters (i.e. surface tension and conductivity); however, for modeling the jet and resulting fiber diameter, the other governing parameters have been shown to be significant contributors (for example, see Refs. [20,21,27–29]).

In this paper, a semi-empirical approach is employed to demonstrate that chain entanglements due to increased polymer concentration or polymer molecular weight can play a vital role in fiber formation during electrospinning. Recently, McKee et al. demonstrated the importance of the entanglement concentration on electrospinning process for linear and branched polyesters [40]. Our approach, while similar, allows a priori prediction of fiber/bead formation as a function of concentration and molecular weight for a variety of polymer/solvent systems. In addition, this approach might be applicable to conventional dry spinning process.

2. Background

Our goal is to explore the importance and establish a correlation between chain entanglements and fiber formation in electrospinning from polymer/solvent systems in the good solvent limit. It well known that for a given molecular weight (M), the entanglement density increases with concentration (ϕ_p, volume fraction of polymer) [41]. Alternatively, the same result is achieved at a fixed polymer concentration by increasing M. Both approaches result in a corresponding increase in solution viscosity (η). As a result, identifying η (solution or zero shear viscosity) as the governing parameter in electrospinning is reasonable; however, it is the effect of ϕ_p and M (through chain entanglements) that are the underlying, fundamental variables (in the good solvent, non-specific polymer–polymer interaction limit). For hydrogen-bonded polymers such as polyamides, even in good solvents, the effect of polymer–polymer interactions on solution viscosity may not be neglected. Similarly, as the solvent quality decreases, effects of polymer–polymer interactions on solution viscosity become increasingly important and must be taken into account [41,42].

Before proceeding with the analysis, a comment with regard to viscosity is instructive. The elongational viscosity (not shear viscosity) is most frequently used to describe the rheological properties of the polymer solution/melt as it is more akin to the deformations being applied during fiber spinning. Since electrospinning is analogous to conventional fiber spinning, the use of elongational viscosity is more appropriate than zero shear viscosity, and in fact, has been recently done by Feng [29]. However, both zero shear and elongational viscosities are a function of the number of chain entanglements (among other factors). Thus a semi-empirical analysis to correlate fiber formation in electrospinning with the number of entanglements will provide a starting point for future research. Subsequent sections provide a brief review of the entanglement effect in melts and solutions and then apply these concepts to the electroprocessing of polymer solutions.

2.1. Entanglements in polymer melts and solutions

Chain entanglements in a melt are essentially the physical interlocking of polymer chains, which is a direct consequence of chain overlap. In a polymer melt, chain overlap, and hence the number of entanglements (or alternatively entanglement density), increases with polymer chain length or molecular weight, M. This is reflected by the dependence of zero shear melt viscosity, η_0, on the molecular weight. At low molecular weights, in the absence of chain entanglements, η_0 is directly proportional to M. Above the critical molecular weight, M_c, corresponding to one entanglement per chain, a distinct upturn in the η_0 versus molecular weight plot is observed [19,41]. The molecular weight dependence of η_0 changes from M^1 to $M^{3.4}$. Without going into details, it suffices to reiterate that M_c refers to the molecular weight corresponding to the onset of entanglement behavior in η_0 while M_e, the entanglement molecular weight, corresponds to the average molecular weight between entanglement junctions (or couples). It is worth noting that physical chain entanglements behave in a similar manner as chemical cross-links, although the chains can slide past one another affecting viscoelastic behavior. Typically, entanglement molecular weights are obtained by viscosity, plateau modulus and/or steady state compliance measurements [19,41]. From a theoretical perspective, Bueche concluded that the ratio of M_c/M_e, corresponding to the number of entanglements, n_e, is ~ 2 [43]. In general, for most polymers, experimental observations suggest this ratio, M_c/M_e, is between 1.7 and 3 [41].

In a polymer solution, both concentration or volume

fraction ϕ and molecular weight M affect the number of chain entanglements. In a dilute solution, below the critical value c^*, chain overlapping is absent. As a result, there are no chain entanglements. At $c=c^*$, chain overlap is initiated and the number of chain entanglements is proportional to c. In general, a relationship between the entanglement molecular weight in solution, $(M_e)_{soln}$, and the melt, M_e, can be made by utilizing the polymer volume fraction (ϕ_p) such that $(M_e)_{soln}=M_e/\phi_p$, which has been validated by numerous experimental observations [19,41]. The critical molecular weight corresponding to the zero shear viscosity follows a similar relationship. The primary effect of solvent is one of dilution. Since the solution concentrations are well above the dilute solution regime ($c \gg c^*$), the effect of solvent quality as expressed using the Mark–Houwink parameter has been neglected in this analysis [41]. Finally, analogous to polymer melts, the solution viscosity exhibits a sharp upturn at a critical molecular weight $(M_c)_{soln}$ where $(M_c)_{soln}/(M_e)_{soln} \sim 2$.

The solution entanglement number $(n_e)_{soln}$ is defined as the ratio of the polymer molecular weight to its solution entanglement molecular weight, i.e. $(n_e)_{soln}=M/(M_e)_{soln}$. For polydisperse systems, the weight-average molecular weight, M_w, is typically used as the molecular weight. Note that for systems with large polydispersity values, arguments for employing the third-moment average molecular weight, M_z, have been made [44]. Accordingly for moderately concentrated or concentrated solutions (i.e. $c \sim c^*$ and $c \gg c^*$, respectively), the entanglement number in solution $(n_e)_{soln}$ can be determined from Eq. (1), below.

$$(n_e)_{soln} = \frac{M_w}{(M_e)_{soln}} = \frac{(\phi_p M_w)}{M_e} \quad (1)$$

The arguments dealing with zero shear viscosity and molecular weight dependence are expected to remain the same; therefore, the upturn in η_0 (M_w^1 to $M_w^{3.4}$) occurs for $(n_e)_{soln} \sim 2$. However, the number of entanglements per chain is given by $(n_e)_{soln}-1$, since an entanglement necessarily involves two chains. Consequently, at $(n_e)_{soln}=2$, there are two entanglements, but only one entanglement per chain.

2.2. Role of entanglements in electroprocessing of polymer–solvent mixtures

During the electroprocessing of polymer solutions, it has been established that an increase in polymer concentration results in the following progression of observed fiber morphology: (1) beads only, (2) beads with incipient fibers, (3) beaded fibers, (4) fibers only and (5) globular fibers/macrobeads. The formation of chain entanglements has been acknowledged as the primary effect in this progression. Fundamentally, electrostatic spraying and spinning of polymer solutions are identical processes with an obvious difference—electrospraying generates droplets/microbeads whereas electrospinning results in fibers. Why is there such a difference in the resulting polymer morphology? Examining the conditions employed for both processes provides a simple explanation: polymer chain overlap is minimal for electrospraying solutions ($c \ll c^*$). From the perspective of the electrospraying community, limiting chain entanglements will help generate smaller droplets and more uniform microbeads. For example, Festag et al. examined the mechanism of inhibiting drop subdivision for dilute polystyrene (PS) solutions [45,46]. Chain entanglements within the drop eventually limit the subdivision of these drops. The mechanism for this process is straightforward. As the solvent evaporates, two competing effects occur: (i) polymer concentration increases and entanglements commence, which stabilizes the droplet from further subdivision and (ii) surface charge increases, which overcomes the droplet surface tension providing a driving force for droplet subdivision. A third factor not to be overlooked is heat transfer due to the rapid evaporation of solvent. This effect will also tend to limit the droplet size: as the droplet is cooled, solvent evaporation slows, skin formation stabilizes the droplets, and surface charge no longer increases.

As the polymer concentration is increased ($c \sim c^*$), a mixture of fibers and beads are observed. In this regime, insufficient chain entanglements are present to fully stabilize the jet. In theory, at even higher polymer concentrations ($c > c^*$), increased chain entanglements can temporarily serve to stabilize the electrospinning jet by inhibiting jet breakup. For dry spinning it has been suggested that above a critical dope (polymer) concentration, the dynamic 'short range' network in the spinning solution is converted to a more stable elastically deformable 'long range' network as the solvent evaporates [34,35,47]. In other words, 'spinnable' solutions exhibit elastic properties [33]. In electrospinning, the existence of a similar mechanism may be invoked. An additional consequence of solvent evaporation is cooling of the jet, which facilitates skin formation and ultimately fiber stabilization. From a fundamental perspective, it is important to understand and be able to predict both the minimum number of entanglements ('short range' entanglement network) in the spinning solution for both fiber initiation (fibers + beads) and complete fiber formation (only fibers). However, since chain disentanglement in the strong elongational flow field is occurring at the same time, exactly how many entanglements are required (so as to form the 'long range' entanglement network as solvent evaporates) is uncertain and is the subject of this paper.

It is here that our previous discussion on the polymer solution viscoelastic behavior is helpful. To recap, as polymer concentration decreases, $(M_e)_{soln}$ increases due to a dilution effect. The solution entanglement number, $(n_e)_{soln}$, can be readily calculated from Eq. (1). The zero shear viscosity exhibits an upturn (M^1 to $M^{3.4}$) for $(n_e)_{soln} \sim 2$, which implies that at least one entanglement per chain is necessary for the viscosity increase. In many instances, the

actual viscosity upturn is a gradual process and begins at $(n_e)_{soln} \leq 2$ and is not finished until $(n_e)_{soln} > 2$. Still, if the fiber initiation can be correlated with a value of $(n_e)_{soln}$ for a variety of polymer/solvent systems and complete fiber formation is also correlated with $(n_e)_{soln}$, then spinnable solutions may be prepared on the basis of a simple calculation.

In subsequent sections, we have used experimental data to show a correspondence between $(n_e)_{soln}$ and fiber formation. The systems chosen for this study are (a) polystyrene (PS)/THF [48], (b) poly(ethylene oxide) (PEO)/H_2O [22,49], (c) poly(D,L-lactic acid) (PDLA)/dimethylformamide (DMF) [50], poly(L-lactic acid) (PLLA)/dichloromethane (DCM) [37], PLLA/chloroform ($CHCl_3$), PLLA/1,1,2,2-tetrachloroethane ($C_2H_2Cl_4$), and (d) poly(vinyl pyrrolidone) (PVP)/ethanol (EtOH). The broad choice of systems allows us to validate our assertion that fiber formation is controlled by $(n_e)_{soln}$ regardless of polymer polarity (non-polar PS versus polar PEO, PVP or PLLA) and even in the presence of strong polymer–solvent interactions (e.g. PEO/water hydrogen bonding). Table 1 lists the entanglement molecular weights for the relevant polymers.

3. Results

3.1. PS/THF

Polystyrene is an amorphous polymer with a glass transition temperature (T_g) around 100 °C. Megelski et al. obtained PS fibers by electrospinning from a variety of solvents including THF [48]. Here, the portion of their results relevant to this study is used. The weight-average molecular weight of PS was 190k (190×10^3gm/mol). The paper provides detailed optical micrographs of bead/fiber formation at 18, 20, 25, 30 and 35 wt% PS, respectively. At 18 wt%, the resulting electroprocessed mats consists of beads only. At 20 wt% PS, structure consisted predominantly of beads with a few incipient fibers. Higher polymer concentrations (25 and 30 wt%) resulted in larger fiber/bead ratios. And finally, at 35 wt%, only fibers were obtained. Therefore, the transition from electrospraying to electrospinning is initiated between 18–20 wt% and completed by 35 wt%.

Employing Eq. (1), the relationship between the calculated $(n_e)_{soln}$ and the transition from electrospraying to electrospinning is evaluated. The entanglement molecular weight of PS is given in Table 1 and obtained from Fetters et al. [51]. Prior to using the values given by Fetters, a correction ($M_e \times 5/4$) is applied to account for the differences in definition of entanglement spacing (Ferry versus Fetters), as suggested by Larson et al. [30]. Thus, M_e of PS is 16.6k, which is in good agreement with the values reported in the literature [19,41]. Fig. 1 plots the calculated $(n_e)_{soln}$ as a function of PS concentration (converted from ϕ_p to wt%) for different molecular weights (50–300k).

Focusing on the 190k plot, three distinct morphology regimes are indicated in Fig. 1: (i) beads only, (ii) fibers + beads and (iii) fibers only. Below 20 wt%, $(n_e)_{soln} < 2$, only beaded morphology is predicted (and observed). It is important to reiterate that experimental observations exhibit a gradual upturn in the viscosity versus M_w (M^1 to $M^{3.4}$), not an abrupt transition. Accordingly, though the transition in Fig. 1 at $(n_e)_{soln} = 2$ is shown as a dotted line, the actual change in morphology from beads to fibers + beads is not as sharp as indicated. In fact, one observes a gradual transformation from beads to elongated beads to a mixture of fibers + beads. Likewise, the transition from fibers + beads to fibers only is a gradual process as less and less beads are observed. At 20 wt% PS, the calculated $(n_e)_{soln}$ is two, which corresponds to an upturn in zero shear viscosity (onset of entanglements). This correlates with the experimental observation of fiber initiation. Even though fiber formation is initiated around 20 wt% PS (corresponding to one entanglement/chain), this is not enough for complete jet stabilization, especially under the influence of the strong elongational flow field. In fact, the observation of fibers and beads for concentrations up to 30 wt% PS supports the

Table 1
Entanglement molecular weights of the polymers considered in this study

Polymer	Entanglement molecular weight ($M_e \times 10^3$ g/mol)
Polystyrene (PS)	16.6
Poly(ethylene oxide) (PEO)	2.1
Poly(L-lactic acid) (PLLA)	8.0
Poly(vinylpyrrolidone) (PVP)	16.8 (estimated)

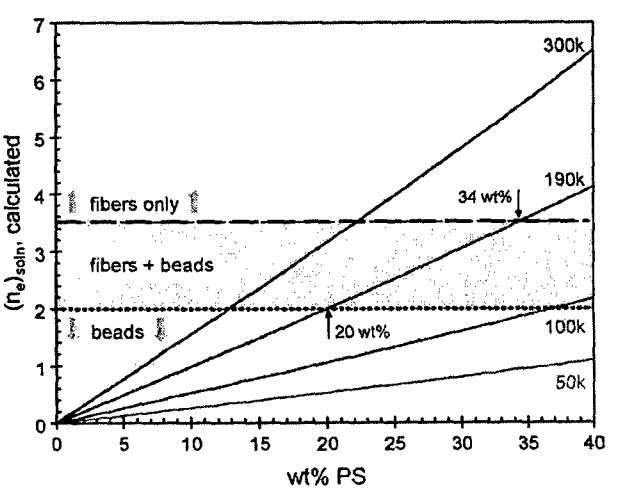

Fig. 1. Plot of the calculated entanglement number $(n_e)_{soln}$ (Eq. (1)) as a function of concentration for PS/THF system. The dashed line indicates the transition for complete fiber formation, i.e. $(n_e)_{soln} = 3.5$, while the dotted line indicates the boundary between beads and a mixture of fibers and beads (shown in fill). Each line represents a different weight-average molecular weight (M_w): 50, 100, 190 and 300k. Arrows indicate the onset of fiber formation (20 wt%) and complete fiber formation (34 wt%) for 190k sample, in agreement with observations (Table 2).

hypothesis of insufficient entanglements for jet stabilization. Continuing further, when the PS concentration is increased to 35 wt%, only fibers are obtained, which corresponds to $(n_e)_{soln}=3.5$ or 2.5 entanglements/chain. The arrow at 34 wt% in Fig. 1, indicates this last transition.

The effect of molecular weight on calculated fiber onset and fiber only transitions is clearly indicated by comparing the 50, 100, 190 and 300k calculations, which show much lower concentration thresholds as the M_w is increased. Moreover, by simply using the entanglement molecular weight (M_e) of the undiluted PS, the electrospinning concentration regime of a known molecular weight PS sample may be predicted and correlated with the onset of entanglements. The more significant question is whether this analysis (based exclusively on chain entanglements) can be applied to other polymer solutions. Moreover, since PS is a non-polar polymer, will this analysis be applicable to polar polymers as well? In an attempt to answer these questions, the semi-empirical entanglement analysis was applied to other systems. The results of the analyses including that of PS/THF are tabulated in Table 2. Also provided in Table 2 are the experimental data for fiber initiation and complete fiber formation obtained from the literature for these systems.

3.2. PLA/DMF or PLA/DCM

Poly(lactic acid), PLA, is a biocompatible/biodegradable linear aliphatic polyester. PLA can be completely amorphous as in the case of poly(D,L-lactide) (PDLA) or semi-crystalline in the case of poly(L-lactide) (PLLA). Zong et al. [50] investigated the effect of processing parameters to make electrospun, bioabsorbable non-woven PDLA membranes for biomedical applications. The weight-average molecular weight of PDLA was 109k and DMF was employed as the solvent. The authors observed that at concentrations <20 wt%, a mixture of large beads and fibers was generated, whereas only fibers were generated on electrospinning solutions between 30 and 35 wt%. Recently, Jun et al. have explored the various parameters important for electrospinning of semi-crystalline PLLA fibers [37]. Dichloromethane (DCM) was the solvent and the polymer molecular weight was 670k (M_w). In contrast to the results of Zong, a mixture of fibers and beads were obtained at concentrations ≤ 1 wt%, and for concentrations ≥ 3 wt%, only fibers were observed. The authors speculated that the large difference in the polymer concentrations required for fiber initiation and complete fiber formation was probably a consequence of the different solvents employed (and by inference, related to solvent volatility effects, $(T_{BP})_{DMF}=153$ °C versus $(T_{BP})_{DCM}=40$ °C).

While the M_e of PLLA is readily available in the literature, no reports on $(M_e)_{PDLA}$ could be found. As a first approximation, the entanglement molecular weights were assumed to be equivalent, $(M_e)_{PDLA}=(M_e)_{PLLA}=8.0$k [52]. Note, by definition, M_e (average molecular weight between entanglements) is primarily a function of chain geometry (architecture) [19,41]. Consequently, despite the large difference in M_w between PDLA and PLLA (109 versus 670k), our assumption that $(M_e)_{PDLA}\sim(M_e)_{PLLA}$ is reasonable; however, the number of entanglements per chain (or solution entanglement number as defined by Eq. (1)) for PLLA will be significantly higher [53,54]. Using the reported value, the polymer concentrations corresponding to fiber initiation, $(n_e)_{soln}=2$, and complete fiber formation, $(n_e)_{soln}=3.5$, were determined for both PDLA/DMF and PLLA/DCM. As shown in Fig. 2 (tabulated in Table 2), our calculations show that for fiber initiation should occur at ~20 wt% for PDLA (109k) and 2.3 wt% for PLLA (670k) while complete fiber formation is expected at 32 wt% for PDLA and 4 wt% for PLLA. The calculated results are in excellent agreement with the experimentally observed values for both PDLA and PLLA. To ascertain whether the large difference in PLLA and PDLA concentrations is truly a molecular weight phenomenon or a solvent effect as suggested by the authors [37], attempts were made to electrospin high molecular weight PLLA ($M_w=670$k) from DMF. The original intent was to validate the entanglement analysis by electrospinning PLLA/DMF solutions; however, PLLA is insoluble in DMF even at elevated temperatures.

Table 2
Summary of results for various polymer/solvent systems

System polymer/solvent	M_w ($\times 10^3$) g/mol	Polymer concentration (wt%) estimated by entanglement analysis		Polymer concentration (wt%) observed experimentally	
		Fiber initiation (fibers+beads) $(n_e)_{soln}\sim 2$	Fibers only $(n_e)_{soln}\sim 3.5$	Fiber initiation (fibers+beads)	Fibers only
PS/THF [48]	190	20	34	18	30–35
PDLA/DMF [50]	109	18.5	32	< 20	30–35
PLLA/DCM [37]	670	2.3	4	< 1	3
PLLA/$CHCl_3$	670	2.0	3.5	–	< 4.1
PLLA/$C_2H_2Cl_4$	670	1.9	3.4	< 3	> 4
PEO/H_2O [56]	400	1.5	2.5	NR	4
PEO/H_2O [20]	2000	0.3	0.8	NR	< 2
PVP/EtOH	1300	4	7.5	3	7–9

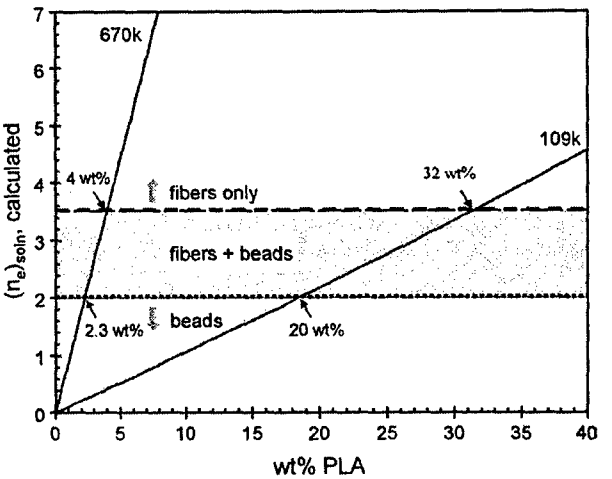

Fig. 2. Plot of the calculated entanglement number $(n_e)_{soln}$ (Eq. (1)) as a function of concentration for PLA/(DMF/DCM) systems. The dashed line indicates the transition for complete fiber formation, i.e. $(n_e)_{soln}=3.5$, while the dotted line indicates the boundary between beads and a mixture of fibers and beads (shown in fill). The lines represent the samples with $M_w=670$ and 109k, and arrows indicate the onset of fiber formation (2.3 and 18.5 wt%) and complete fiber formation (4 and 31 wt%) for the 670 and 190k samples, respectively.

Nevertheless, based on preliminary electrospinning experiments performed in other chlorinated solvents of differing volatility [55], it appears that the variation in the critical concentration between the studies of Jun and Zong may be attributed to the large M_w differences (670 versus 109k) of the samples more than differences in solvent volatility. Still, the extreme volatility of DCM may make a minor contribution to the observation of fiber onset at lower concentrations.

3.3. PEO/H_2O

Polyethylene oxide is a semi-crystalline linear aliphatic polyether with a low T_m (65 °C). Dietzel et al. [56] have examined the effect of processing variables including concentration on electrospinning of PEO in H_2O. The authors observed that for 4–10 wt% PEO ($M_w=400$k) only fibers were produced. Below this critical concentration (4 wt%), a mixture of fibers and beads were obtained. In another study by Shin et al. [22], 2 wt% PEO ($M_w=2000$k) was deliberately chosen to ensure that only fibers were produced, which implies the critical concentration corresponding to complete fiber formation is <2 wt%. The PEO/H_2O system gives us an opportunity to apply the entanglement analysis, where strong polymer/solvent interactions (hydrogen bonding between PEO ether groups and hydroxyl groups in H_2O) are known to exist.

Table 1 gives $(M_e)_{PEO}$ obtained from literature [51] by applying the proper correction ($M_e\times5/4$). The comparison between experimental data and predicted values are given in Table 2. Entanglement analysis predicts that for $M_w=400$k, and concentrations >2.5 wt% only fibers should be obtained, while for a 2000k sample the corresponding concentration is 0.8 wt%. Experimentally, Deitzel et al. observed a critical concentration of 4 wt%—whether the presence of strong specific interactions between PEO and H_2O is the cause of this discrepancy between calculated and observed fibers is unclear at this time. In addition, fiber initiation is expected to be at ~1.5 wt%, which cannot be confirmed since the authors did not report the PEO wt% for fiber initiation. For the 2000k sample, at 2 wt%, the concentration employed by Shin, one is well above minimum concentration for complete fiber formation. The concentration for fiber initiation is predicted to be ~0.3 wt%. Hence, a mixture of fibers and beads should be obtained for concentrations between 0.3 and 0.8 wt% PEO. Lacking experimental data to confirm this prediction, validation of predicted fiber onset was attempted by electrospinning a 0.4 wt% PEO solution ($M_w=2000$k) in H_2O [57]. Electrospinning predominantly resulted in bead formation; however, close inspection of the glass slide showed some incipient fibers, which consisted of beads attached to one another (Fig. 3). At this low concentration, PEO beads cover most of the slide. Evidently, 0.4 wt% PEO/H_2O solutions are near the threshold for fiber onset in agreement with the entanglement analysis.

The simple entanglement analysis clearly demonstrates that the viscosity transition, i.e. $(n_e)_{soln}\sim2$, corresponds to fiber initiation while $(n_e)_{soln}\sim3.5$ corresponds to complete fiber formation. In addition, this analysis is valid not just for non-polar polymer/solvent systems but also where polymer–solvent hydrogen bonds are involved. The good agreement between the experimental observations and the predictions clearly illustrate the role played by entanglements in the electrospinning process for the good solvent case. So far, this approach has been validated using experimental observations published in the literature on polymers with reported M_e values. In the next section (and as a further test of this approach), a system for which no prior detailed experimental data are available is examined (including no reported M_e values).

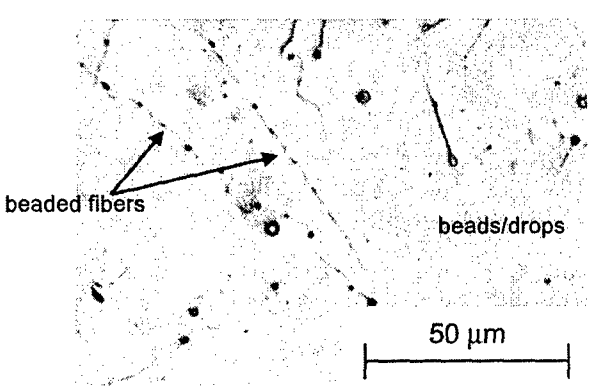

Fig. 3. Optical micrograph of the structures obtained by electrospinning 0.4 wt% PEO ($M_w=2000$k) in deionized H_2O. Note the presence of beads and beaded fiber morphology.

3.4. PVP/EtOH

Poly(vinyl pyrrolidone) is an amorphous polymer that may form hydrogen bonds to protic solvents such as alcohols. Recently, Yang et al. [58] and Li et al. [59] obtained fibers by electrospinning PVP in EtOH, DMF and an EtOH/DMF mixture. However, in both instances, no information on the concentration dependence of fiber initiation and/or fiber formation was presented. Consequently, the PVP/EtOH system was chosen to provide further substantiation of the entanglement analysis. In the absence of any report on the entanglement molecular weight for PVP, $(M_e)_{PVP}$, an estimated value of $(M_e)_{PVP}$ was determined using the entanglement constraint model [51]. According to Fetters, the M_e of a polymers is a function of the characteristic ratio (C_∞), the average molecular weight per backbone bond (m_o), bond length (l_o) and density (ρ). The precise dependence is given in Eq. (2), below:

$$M_e \propto C_\infty^{-3} m_o^3 l_o^{-6} \rho^{-2} \quad (2)$$

Using the above relationship, the value of the $(M_e)_{PVP}$ can be estimated by comparing to a reference polymer possessing similar topological structure. In this case, PS is chosen as the reference thereby eliminating l_o as a variable (since $(l_o)_{PS} \sim (l_o)_{PVP}$). The characteristic ratios of PVP reported in the literature have generally been obtained in solution and vary significantly [60,61]. For example, $C_{\infty(PVP/H2O)} = 14$ while $C_{\infty(PVP/EtOH-H2O)} = 12.3$; in this case, the calculated value of $C_{\infty(PVP)} \sim 11$ is selected [61]. Other parameters employed for the calculation (Eq. (2)) include $C_{\infty(PS)} = 10.8$; $\rho_{PS} = 1.06$ g/cm^3; $\rho_{PVP} = 1.13$ g/cm^3 [62]. Employing $(M_e)_{PS} = 16.6$k as given in Table 1, $(M_e)_{PVP}$ was estimated using Eq. (2) to be 16.8k. The similarity of the M_e values for PS and PVP is not surprising since chain entanglements are predominantly a function of topology. Using $M_w = 1300$k, Eq. (1) is employed to calculate the polymer concentration required for fiber initiation and complete fiber formation and is reported in Table 2. Accordingly, fiber initiation is predicted to commence at 4 wt% while only fibers should be obtained for PVP concentrations ≥ 7.5 wt%. Between these two concentration limits, a mixture of fibers and beads is predicted.

Based on these calculations, PVP/EtOH solutions with 1, 3, 7 and 9 wt% polymer, respectively, were prepared and electrospun while keeping the other control parameters such as applied voltage, flow-rate and source-to-target distance constant [57]. Optical micrographs in Fig. 4 clearly show at 1 wt% polymer (Fig. 4(A)), the structure is predominantly one of elongated beads. As PVP concentration is increased to 3 wt% (Fig. 4(B)), the presence of a few electrospun fibers becomes apparent though the dominant morphology is beads. Thus fiber initiation occurs around 3 wt% that is in reasonable agreement with the predicted value (4 wt%). At 7 wt% (Fig. 4(C)), the morphology is essentially fibers, with some fibers having a beaded morphology. The critical concentration for complete fiber formation is slightly higher than 7 wt%, which does not corroborate the results of Yang wherein smooth nanofibers of PVP in EtOH were obtained at 4 wt% [58]. To eliminate electric field as a possible reason for this discrepancy, the effect of electric field on fiber morphology for a concentration of 7 wt% was examined (not shown in figure). Beaded fiber morphology was obtained for voltages from 12 to 20 kV keeping the source-to-target distance constant at 12 cm. A probable cause for the disagreement could be the mode of collection of the fibers/beads [63]. An alternative explanation might be the presence of titanium tetraisopropoxide in the solutions used by Yang, which could alter the critical concentration for complete fiber formation. However, at the present time, this is purely speculative and the precise reason(s) for the discrepancy is still not fully resolved. In our case, as the PVP concentration is increased to 9 wt%, a completely fibrous network is obtained as shown in Fig. 4(D). This is in excellent agreement with calculations. Summarizing, fiber initiation occurs around 3 wt%, from 3 to 7 wt% a mixture of fibers + beads are observed, and at 9 wt%, only fibers are obtained. This example clearly illustrates the importance of the entanglement analysis even in the absence of reliable M_e values.

4. Discussion

4.1. Universality of the model

By predicting fiber/bead formation for various systems, the validity of an entanglement analysis is clearly demonstrated. The present analysis requires calculation of $(n_e)_{soln}$, which varies with the molecular weight, M_w. Alternatively, one can employ the Simha–Frisch parameter $= c[\eta]$ (also referred to as the Berry number) to describe the degree of chain overlap in a solution [64]. Recently, Koski et al. [65] employed this type of analysis to predict complete fiber formation. The approach that we have outlined, valid for the good solvent case in the absence of strong interactions permits the prediction of bead/fiber formation apriori without the necessity of any experiments. Furthermore, the dependence of viscosity (chain entanglements in this case) on $c[\eta]$ is believed to be a result of the equivalent sphere hydrodynamics; consequently, it is valid for low polymer concentrations. At higher concentrations, a fundamentally different type of intermolecular interaction dependent on $(\phi_p M_w)$ rather than $c[\eta]$, is more relevant [41]. In electrospinning, the required polymer concentrations are generally in the semi-dilute ($c \gg c^*$) regime; hence the product, $\phi_p M_w$, is more appropriate in this instance. Fig. 5 shows a plot of this type for the PEO/H_2O system. Based on the previously discussed value of $(n_e)_{soln} \sim 2$, the graph predicts that a mixture of fibers + beads is obtained as long as $\phi_p M_w \geq 4.2$k. On the other hand, for $\phi_p M_w \geq 7.4$k, the

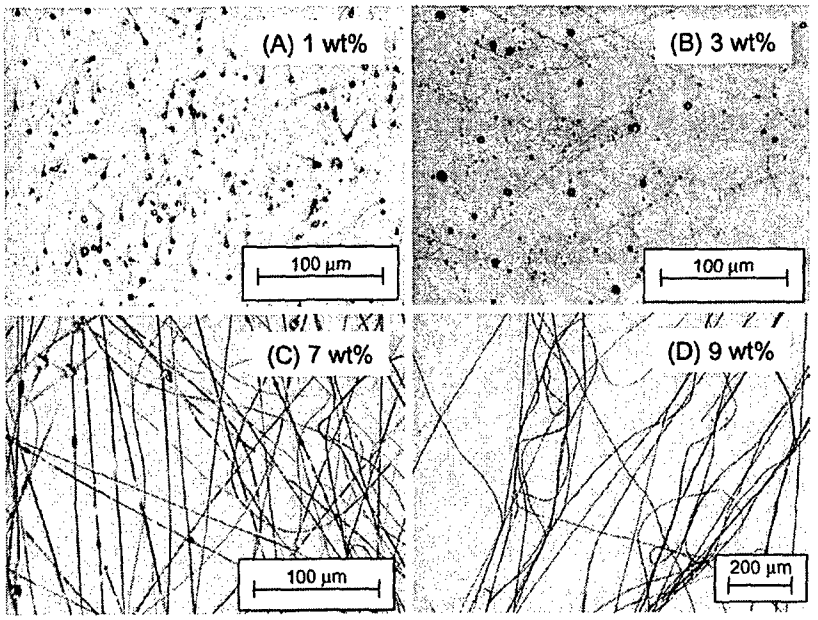

Fig. 4. Optical microscopy of structures obtained by electrospinning PVP/EtOH solutions at different concentrations of PVP (M_w=1300k). (A) 1 wt%, elongated beads; (B) 3 wt%, incipient fiber formation; (C) 7 wt%, beaded fibers and fibers; and (D) 9 wt%, fibers only.

graph predicts only fibers should be obtained, which is confirmed by experiment. Therefore for PEO/H_2O electrospinning, the value of $\phi_p M_w$ (7.4k) at which the electrospraying to electrospinning transition occurs implies that the critical PEO concentrations can be prepared with just the knowledge of the weight-average molecular weight of PEO. These critical $\phi_p M_w$ values are valid for PEO only (since the slope of the line in Fig. 5 is $1/M_e$), but similar plots can be developed for other polymers.

One way to standardize the above treatment for other polymers may be by using the definition of $(n_e)_{soln}$. For initiation of fibers, i.e. $(n_e)_{soln}=2$, and $\phi_p M_w = 2M_e$. On the other hand, for complete fiber formation, $(n_e)_{soln} \geq 3.5$, or $\phi_p M_w \geq 3.5\ M_e$. Thus with the knowledge of the entanglement molecular weight (M_e) and the weight-average molecular weight (M_w) for a given polymer, one may predict a priori the polymer concentrations (ϕ_p) required to move through the electrospraying/electrospinning transition.

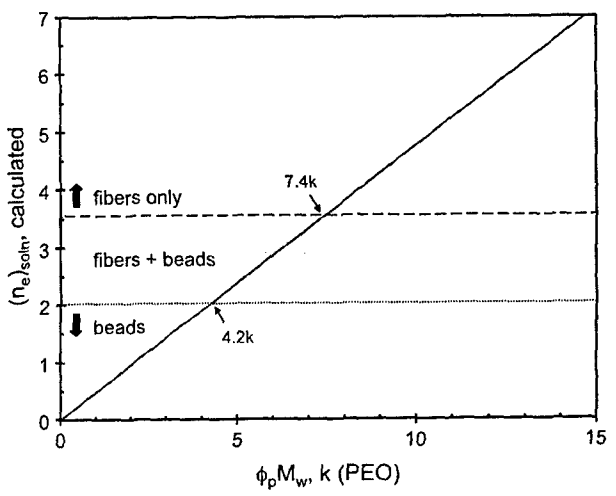

Fig. 5. Calculated $(n_e)_{soln}$ for PEO/H_2O as a function of ($\phi_p M_w$). The slope of the plot is $1/M_e$, and the arrows indicate fiber onset and fiber only morphologies at $\phi_p M_w$=4.2 and 7.4k, respectively.

4.2. Comments on relationship between $(n_e)_{soln}$ and fiber/bead formation

From a fundamental perspective, as discussed previously in this paper, the volume fraction ϕ_p or molecular weight M_w at which fiber initiation occurs corresponds to the sharp upturn (M_w^1 to $M_w^{3.4}$) in the $\eta - M_w$ plot, i.e. $(n_e)_{soln} \sim 2$ (number of entanglements/chain = 1). Experimental evidence demonstrates that increasing ϕ_p or M_w results in a mixture of fibers and beads. Eventually above a certain critical ϕ_p or M_w value, only fibers are obtained. Our analysis based on experimental data suggests that the $(n_e)_{soln}$ value corresponding to this transition is $\sim$3.5, which is equivalent to about 2.5 entanglements/chain. Interestingly, in early work, Schreiber et al. [66] and Hayahara et al. [67] suggested that in polymer melts or concentrated solutions, there exists a critical M_w or ϕ_p, above which an elastically deformable entanglement network is obtained. For concentrated acrylonitrile–methyl acrylate copolymer solutions, it was concluded that the minimum number of entanglements required to form this elastic network is $\sim$3 [67], which corresponds to $(n_e)_{soln} \sim 4$. In the electrospinning process, our analysis suggests that chain entanglements appear to stabilize the ejected liquid jet long enough for solvent

evaporation to occur and form an elastically deformable 'long range' network, which ultimately yield fibers. Note that it is well known that for a much more extensive elastic network $(n_e)_{soln} \geq 6$–8, the steady state compliance, J_e^0, becomes independent of M_w [19,41]. Summarizing, in good solvents, fiber initiation corresponds to the onset of entanglements whereas there is a direct correlation between complete fiber formation and the onset of a deformable elastic network due to chain entanglements.

In principle, this could imply the existence of a critical M_w below which fiber formation in good solvents may not be possible by electrospinning despite the presence of three of more entanglements per chain. For example, one can envision low molecular weight polymer solutions with $(n_e)_{soln} \sim 4$ at high polymer ϕ_p, where establishing a deformable elastic network may be difficult due to lower relaxation or disentanglement time (τ_D). It is well known that a long chain (higher M_w) needs more time to disentangle than a shorter chain (low M_w). According to the reptation model, $\tau_D \sim M_w^{3.4}$. This can result in significant entanglement loss for low molecular weight polymers in fast flowing systems or under elongational flow such as occurring in electrospinning [68–70]. A critical parameter, which affects the disentanglement of chains, is the applied strain rate ($\dot{\varepsilon}$). The presence of the physical junctions per se does not ensure formation of a mechanical or elastic network due to chain disentanglement. Only under the influence of a shear stress or elongational flow, as is the case for electrospinning, does there exist a critical strain rate (greater than the disentanglement or reptation time), above which the entanglements or physical junctions act as mechanical effective junctions on short time scales ($> \tau_D$) [71]. An appropriate parameter to include these effects (τ_D, $\dot{\varepsilon}$) is the Deborah number (De) as done by Feng [29]. Finally another factor to consider is the extensibility of the chain between the entanglement junctions [72]. For an equal number of entanglements/chain (e.g. three or more for fiber formation in electrospinning), the extensibility would be lower as M_w decreases, which together with a faster disentanglement time would result in significantly reduced elastic forces. In this situation, beads or beaded fibers may be obtained. Work is currently underway in our laboratory to test this hypothesis.

4.3. Fiber formation: effect of other factors

The entanglement analysis clearly shows that in good solvents chain entanglements can act as a stabilizing influence on the ejected jet promoting fiber formation. However, there are other factors that can influence the fiber formation. Among them, the applied voltage and surface tension are two very important parameters, which affect both the Taylor cone and fiber/bead formation. As a starting point, a dimensionless electrospinning number $Vq/\gamma R^2$, defined as the ratio of the electrical energy (Vq) to the surface free energy (γR^2), is introduced. This ratio was specifically chosen since the electrical energy is the driving force for ejection of the jet from the Taylor cone while the surface free energy is the force opposing the jet ejection. Note that $Vq/\gamma R^2$ is quite similar to the electric Bond number [73,74]. Thus, during the electrospinning process, a jet of liquid is ejected from the Taylor cone if $Vq/\gamma R^2 > 1$, i.e. as the electrical energy (Vq) overcomes the surface free energy (γR^2). In addition to the critical voltage needed for the ejection of liquid from the Taylor cone, it is well known that as the voltage (and hence Vq) is increased, the morphology changes from beads to beaded fibers to only fibers. However, further voltage increase can affect cone stability, which can result in the formation of defective (beaded) fibers [56]. An alternate way to obtain fibers is to lower surface tension (and hence γR^2) by adding a surfactant [75]. Thus, qualitatively, the dimensionless number $Vq/\gamma R^2$ may be used to explain the morphologies obtained by electrostatic processing. However, one needs to be extremely careful in using the electrospinning number since $Vq/\gamma R^2$ may be a function of other parameters such as chain entanglements, solvent volatility, flow rate, humidity, and temperature. An in-depth dimensional analysis is being performed to obtain the precise relationships of the various parameters to the electrospinning number and will be the subject of a future paper. Here we simply present some conceptual arguments on the usefulness of the electrospinning number and importance of other factors for determining fiber formation.

4.3.1. Solution conductivity

Jun et al. have shown that increasing solution conductivity by addition of a salt can significantly aid fiber formation [37]. As discussed earlier, a mixture of fibers and beads was obtained by electrospinning a 2 wt% PLLA ($M_w = 670$k) solution from DCM. However, addition of a salt, such as pyridinium formate (PF), enables fiber formation at lower concentrations. For example, by addition of 0.8 wt% PF (with respect to DCM) to a 2 wt% polymer solution, only fibers were obtained. From the entanglement analysis perspective, at 2 wt%, $(n_e)_{soln} < 2$ and hence we expect only beads. While addition of the salt should not change the entanglement number, it has a positive effect on the electrospinning number. Specifically, the electrical energy (Vq) increases. On the other hand, the change in surface free energy (γR^2) due to change in surface tension is not expected to be significant [37]. Thus fiber formation is promoted at lower concentrations, the stabilizing factor being the increased electrical energy [20,21] and not chain entanglements.

One can also disrupt fiber formation by lowering the electrical energy as done by Fong et al. for PEO/water [76]. The authors investigated the effect of neutralizing ions generated by a corona discharge on the morphology of the PEO fibers. In the absence of the discharge, only fibers were obtained. However in the presence of the discharge, beaded fibers were formed. The amount of beads was proportional

to the corona discharge voltage. In this case as the authors suggest the electrical forces (and hence the electrospinning number $Vq/\gamma R^2$) stabilizing the ejected jet is reduced by the neutralizing ions thereby destabilizing the jet. Note that in both the cases discussed above, though the number of entanglements is unchanged, the electrospinning number is altered due to changes in the electrical energy term.

4.3.2. Solvent quality

While the examples considered in this paper clearly show that chain entanglements are important, it should be reiterated that this is valid for good solvents under normal operating conditions. As mentioned earlier, it was assumed that polymer–polymer interactions are not significant enough to affect solution viscosity. Consequently, solvent quality is not an issue and electrospinning PLLA or PDLA from DMF or DCM does not alter model predictions or experimental observations. However, it has been shown that addition of another solvent can dramatically alter the concentration needed for fiber formation. For example, work in our laboratory by Bates et al. suggests that addition of acetone to a PVDF solution (M_w=180k) in DMF significantly lowers the critical concentration necessary for fiber formation [77]. In this case, acetone is a marginal solvent for PVDF as indicated by the polymer–solvent interaction parameters ($\chi_{PVDF/acetone}$=0–0.1 versus $\chi_{PVDF/DMF}$=−0.4) [78]. In fact, in pure acetone, fibers can be obtained at concentrations as low as 7.5 wt%. Employing our analysis, a concentration of 30 wt% PVDF is calculated to obtain electrospun fibers (for 180k PVDF in DMF—a good solvent). The issue of solvent quality can be quite complex and is outside the scope of this work. However, here we lay the groundwork for future experiments by summarizing our ideas using the example of a polymer/solvent system previously reported by our laboratory.

Kenawy et al. [38] obtained fibers by electrospinning ethylene vinyl alcohol copolymers containing 56–71 wt% vinyl alcohol in rubbing alcohol (*v/v*, 70/30 2-propanol/water). Since the copolymer is partially crystalline, application of heat (80 °C) was a prerequisite to completely dissolve the copolymer and obtain a homogenous solution. After cooling to room temperature, electrospinning results in EVOH fibers. The EVOH/rubbing alcohol solution phase behavior is quite complex since it has been clearly demonstrated that both solid/liquid (crystallization) and liquid/liquid phase separation (upper critical solution temperature, UCST) occurs in this system, albeit quite slowly [79]. In fact, the polymer eventually precipitates if left for any prolonged period at room temperature suggesting complete phase separation. Thus the presence of micro- and/or nanoscopic crystallite junctions or 'embryonic nucleation sites', together with the proximity of the UCST, may in fact promote the electrospinning process and subsequent fiber formation. We have preliminary evidence to suggest that a similar process may occur in the case of PVDF in acetone (except for the absence of UCST) and will report on this work in a forthcoming contribution [80].

Another factor that can promote fiber formation is the enhancement of polymer–polymer interactions due to presence of inter-chain hydrogen bonding [81,82]. This is clearly demonstrated by the fiber formation of low molecular weight Nylons (M_w<25k) at low concentrations (2.5 wt%) in contrast to polymers where no hydrogen bonding is present [81].

4.3.3. Fiber diameter

Another area of interest is the prediction of fiber diameter and more importantly the dependence of this diameter on the concentration/molecular weight space. For a given molecular weight, it is well known that fiber diameter increases with polymer concentration. Similar results are observed for fixed concentrations with increasing molecular weights. From our perspective, we are interested in the ability to a priori predict the concentration/molecular weight space for the spinning of nanometer size fibers as opposed to micron size fibers. Using the entanglement analysis we can now formulate a qualitative picture. For lower molecular weight polymers, to satisfy the entanglement consideration [entanglement number=$(n_e)_{soln}$=3.5] in order to obtain only fibers, a higher polymer chain concentration per unit volume would be required which leads to lower extensibility. On the other hand, for high molecular weight polymers, due to the length of each chain, a lower chain concentration per unit volume would be needed to satisfy the entanglement consideration. The lower number of chains per unit volume should directly translate to lower fiber diameters due to large chain extensibility. This argument is currently under investigation and results will be reported in the near future. This is conceptually in agreement with the suggestion by McKee et al. [40] who demonstrated that the fiber diameter could be universally scaled with the normalized concentration (to the entanglement concentration) to the 2.6 power.

5. Conclusions

In the present paper, we believe that we have demonstrated the importance of entanglements for fiber formation in polymer/good solvent systems. In addition, we have proposed a straightforward methodology to apriori predict fiber formation in good solvents. The only required parameter is the entanglement molecular weight of the undiluted polymer (M_e). In general, M_e is readily available for a large number of polymers (~70 or more). Alternatively, in the absence of experimental values, M_e can also be theoretically estimated (as we have done for PVP) by employing the entanglement constraint model. Then, based on the structure requirements (fibers/beads/mixture), our predictions facilitate the proper choice of polymer concentration/molecular weight space.

Acknowledgements

The authors would like to thank Prof John Rabolt and Dr Joseph Dietzel of the University of Delaware for providing information on the absence of solvent evaporation close to the needle. Additionally, the authors would like to thank Prof Gareth H. McKinley for discussions on entanglements and elongational viscosity. We also thank B.I. (Boehringer Ingelheim) Chemicals for donating samples of poly(L-lactide acid) (M_w=670k). The authors would also like to thank DARPA (Bio-Optic Synthetic Systems Program) and the NASA Office of Space Sciences for generous support.

References

[1] Doshi J, Reneker DH. J Electrostat 1995;35:151–60.
[2] Srinivasan G, Reneker DH. Polym Int 1995;36:195–201.
[3] Reneker DH, Chun I. Nanotechnology 1996;7:216–23.
[4] Frenot A, Chronakis IS. Curr Opin Colloid Interface Sci 2003;8:64–75.
[5] Huang ZM, Zhang YZ, Kotaki M, Ramakrishna S. Compos Sci Technol 2003;63:2223–53.
[6] Layman JM, Kenawy E-R, Watkins JR, Carr Jr ME, Bowlin G, Wnek GE. Polym Prepr 2003;44:94–5.
[7] Barris MA, Zelinka RL. US Patent No. 4,650,506. Issued March 17; 1987 to Donaldson Company, Inc.
[8] Chung HY, Hall JRB, Gogins MA, Crofoot DG, Weik TM. US Patent No. 6,743,273. Issued June 1; 2004 to Donaldson Company, Inc.
[9] Kenawy ER, Bowlin GL, Mansfield K, Layman J, Simpson DG, Sanders EH, et al. J Control Release 2002;81:57–64.
[10] Gibson P, Schreuder-Gibson H, Rivin D. Colloids Surf A 2001;187:469–81.
[11] Schreuder-Gibson H, Gibson P, Senecal K, Sennett M, Walker J, Yeomans W, et al. J Adv Mater 2002;34:44–55.
[12] Boland ED, Matthews JA, Pawlowski KJ, Simpson DG, Wnek GE, Bowlin GL. Front Biosci 2004;9:1422–32.
[13] Matthews JA, Wnek GE, Simpson DG, Bowlin GL. Biomacromolecules 2002;3:232–8.
[14] Li WJ, Laurencin CT, Caterson EJ, Tuan RS, Ko FK. J Biomed Mater Res 2002;60:613–21.
[15] Taylor G. Proc R Soc London A, Mat Phys Sci 1964;280:383–97.
[16] Reneker DH, Yarin AL, Fong H, Koombhongse S. J Appl Phys 2000;87:4531–47.
[17] Shin YM, Hohman MM, Brenner MP, Rutledge GC. Appl Phys Lett 2001;78:1149–51.
[18] Theron SA, Zussman E, Yarin AL. Polymer 2004;45:2017–30.
[19] Ferry JD. Viscoelastic properties of polymers. New York: Wiley; 1980 p. 641.
[20] Hohman MM, Shin M, Rutledge G, Brenner MP. Phys Fluids 2001;13:2201–20.
[21] Hohman MM, Shin M, Rutledge G, Brenner MP. Phys Fluids 2001;13:2221–36.
[22] Shin YM, Hohman MM, Brenner MP, Rutledge GC. Polymer 2001;42:9955–67.
[23] Spivak AF, Dzenis YA. Appl Phys Lett 1998;73:3067–9.
[24] Spivak AF, Dzenis YA, Reneker DH. Mech Res Commun 2000;27:37–42.
[25] Yarin AL, Koombhongse S, Reneker DH. J Appl Phys 2001;90:4836–46.
[26] Yarin AL, Koombhongse S, Reneker DH. J Appl Phys 2001;89:3018–26.
[27] Fridrikh SV, Yu JH, Brenner MP, Rutledge GC. Phys Rev Lett 2003;90:144502.
[28] Feng JJ. Phys Fluids 2002;14:3912–26.
[29] Feng JJ. J Non-Newtonian Fluid Mech 2003;116:55–70.
[30] Larson RG, Sridhar T, Leal LG, McKinley GH, Likhtman AE, McLeish TCB. J Rheol 2003;47:809–18.
[31] Blades H, White JR. US Patent No. 3,081,519. Issued March 19; 1963 to E.I. du Pont de Nemours and Co.
[32] Shin H, Guckert JR, Kurian JV. US Patent No. 6,458,304. Issued October 1; 2002 to E.I. du Pont de Nemours and Co.
[33] Ziabicki A. Fundamentals of fibre formation: The science of fibre spinning and drawing. New York: Wiley; 1976. p. 488.
[34] Gou ZM, McHugh AJ. J Appl Polym Sci 2003;87:2136–45.
[35] Gou ZM, McHugh AJ. J Non-Newtonian Fluid Mech 2004;118:121–36.
[36] Gupta P, Wilkes GL. Polymer 2003;44:6353–9.
[37] Jun Z, Hou HQ, Schaper A, Wendorff JH, Greiner A. E-Polymer 2003; No. 009.
[38] Kenawy ER, Layman JM, Watkins JR, Bowlin GL, Matthews JA, Simpson DG, et al. Biomaterials 2003;24:907–13.
[39] Stephens JS, Frisk S, Megelski S, Rabolt JF, Chase DB. Appl Spectrosc 2001;55:1287–90.
[40] McKee MG, Wilkes GL, Colby RH, Long TE. Macromolecules 2004;37:1760–7.
[41] Graessley WW, editor. Advances in polymer science, vol. 16. New York: Springer; 1974. p. 179.
[42] Gandhi KS, Williams MC. J Appl Polym Sci 1972;16:2721–5.
[43] Bueche F. J Chem Phys 1956;25:599–600.
[44] Bueche F. J Polym Sci 1960;53:527–30.
[45] Festag R, Alexandratos SD, Joy DC, Wunderlich B, Annis B, Cook KD. J Am Soc Mass Spectrosc 1998;9:299–304.
[46] Festag R, Alexandratos SD, Cook KD, Joy DC, Annis B, Wunderlich B. Macromolecules 1997;30:6238–42.
[47] Griswold PD, Cuculo JA. J Appl Polym Sci 1974;18:2887–902.
[48] Megelski S, Stephens JS, Chase DB, Rabolt JF. Macromolecules 2002;35:8456–66.
[49] Deitzel JM, Kleinmeyer JD, Hirvonen JK, Tan NCB. Polymer 2001;42:8163–70.
[50] Zong XH, Kim K, Fang DF, Ran SF, Hsiao BS, Chu B. Polymer 2002;43:4403–12.
[51] Fetters LJ, Lohse DJ, Richter D, Witten TA, Zirkel A. Macromolecules 1994;27:4639–47.
[52] Cooper-White JJ, Mackay ME. J Polym Sci, B: Polym Phys 1999;37:1803–14.
[53] Since M_e is a function of chain geometry, subtle changes in polymer structure (PLLA versus PDLA) can alter M_e. For example, the viscoelastic properties and, consequently, M_e, of syndiotactic polypropylene (PP) have been found to be quite different from atactic and isotactic PP (Ref. [54]). Still, in the absence of accurate $(M_e)_{PDLA}$ values, the assumption of equivalent entanglement molecular weights for PDLA and PLLA are more than likely reasonable to a first approximation
[54] Jones TD, Chaffin KA, Bates FS, Annis BK, Hagaman EW, Kim MH, et al. Macromolecules 2002;35:5061–8.
[55] Since PLLA was found to be insoluble in DMF, other solvents were examined. PLLA solutions were prepared using three different solvents: 5 wt% in DCM, 4 wt% in $CHCl_3$ (T_{BP}=61 °C) and 4 wt% in 1,1,2,2-tetrachloroethane (TCE, T_{BP}=147 °C). For the PLLA/TCE system, at 4 wt% mostly fibers with some beads were observed. In contrast, complete fibers are obtained from DCM (5 wt%) and $CHCl_3$ (4 wt%). The results are included in Table 2. It was also noticed that for the PLLA/TCE system, besides the beaded fibers, globular polymer droplets (100 μm) were observed, indicative of poor solubility. This is believed to be a result of the lower affinity of PLLA and TCE (in comparison to DCM and $CHCl_3$), which results in

a much slower dissolution rate of PLLA. In a subtle manner, though fibers are obtained, PLLA electrospinning is nevertheless affected by solvent quality

[56] Deitzel JM, Kleinmeyer J, Harris D, Tan NCB. Polymer 2001;42: 261–72.

[57] For details of the experimental setup see Ref. [38]. PEO (M_w= 2000k), PVP (M_w=1300k), and EtOH (200 proof, HLPC grade) were all obtained from Aldrich and used as received. For the electrospinning experiment, a 0.4 wt% PEO solution in distilled deionized H_2O was prepared. PVP/EtOH solutions of different concentrations were also prepared (1, 3, 7 and 9 wt%—these concentrations were chosen based on theoretical predictions as discussed in the text). In a typical experiment, a solution of polymer (PEO/H_2O or PVP/EtOH) was drawn into a disposable polypropylene syringe equipped with a blunted stainless steel syringe tip. Employing a syringe pump (kdScientific, New Hope, PA) to generate a constant flow-rate (5 mL/h), the syringe tip was connected to a high voltage power supply (CZE 1000R, Spellman, NY). For the PEO/H_2O system, the field strength employed by Shin et al. (Ref. [22]) was employed: the applied voltage =17 kV and the source-to-target distance =20 cm. For the PVP/EtOH system, the source-to-target distance = 10 cm and an applied voltage of 10 kV was required for a jet of liquid to eject; consequently, an applied voltage = 12 kV was used in the PVP/EtOH experiments. Fibers for visualization by optical microscopy were collected on glass slides covering a grounded metal target rotating at approximately 300–500 rpm. Optical micrographs were obtained using an Olympus optical microscope (Olympus BE201).

[58] Yang Q, Li Z, Hong Y, Zhao Y, Wang C, Qiu S, et al. Polym Prepr 2003;44:173.

[59] Li D, Xia YN. Nano Lett 2003;3:555–60.

[60] Brandrup J, Immergut EH, Grulke EH. Polymer handbook. New York: Wiley; 1999.

[61] Tarazona MP, Saiz E. J Biochem Biophys Methods 2003;56:95–116.

[62] Obtained from the Pharmaceutical Technology Report(PTR-005-1) published by Hercules Incorporated.

[63] In our case fibers/beads are obtained for visualization by optical microscopy by collecting samples on glass slides covering a grounded metal target rotating at approximately 300–500 rpm. During imaging, the entire microscope slide is scanned for the presence of fibers, beaded fibers or just beads. In contrast, Yang et al. have mounted a TEM copper grid on top of an Al foil, which acts as the cathode. We believe there is a distinct possibility of underestimating the critical concentration required for complete fiber formation using this technique, since fibers will be preferentially trapped on the grid. This is especially true when the number of fibers having a beaded morphology is quite low as is the case in this system for solutions ranging from 5 to 7 wt%.

[64] Frisch HL, Simha R. In: Eirich FR, editor. Treatise on rheology, vol. 1. New York: Academic Press; 1956.

[65] Koski A, Yim K, Shivkumar S. Mater Lett 2004;58:493–7.

[66] Schreiber HP, Rudin A, Bagley EB. J Appl Polym Sci 1965;9:887–92.

[67] Hayahara T, Takao S. J Appl Polym Sci 1967;11:735–46.

[68] Hua CC, Yang CY. J Polym Res Taiwan 2002;9:79–90.

[69] Mead DW, Larson RG, Doi M. Macromolecules 1998;31:7895–914.

[70] Mhetar VR, Archer LA. J Polym Sci, B: Polym Phys 2000;38:222–33.

[71] Keller A. Faraday Discuss 1995;1–49.

[72] Rothstein JP, McKinley GH. J Non-Newtonian Fluid Mech 2002;108: 275–90.

[73] Basaran OA, Scriven LE. J Colloid Interface Sci 1990;140:10–30.

[74] Gonzalez H, Castellanos A. J Fluid Mech 1993;249:185–206.

[75] Yao L, Haas TW, Guiseppi-Elie A, Bowlin GL, Simpson DG, Wnek GE. Chem Mater 2003;15:1860–4.

[76] Fong H, Chun I, Reneker DH. Polymer 1999;40:4585–92.

[77] Bates WD, Barnes CP, Ounaies Z, Wnek GE. Polym Prepr 2003;44: 114.

[78] Tazaki M, Wada R, Okabe M, Homma T. Polym Bull 2000;44: 93–100.

[79] Young TH, Cheng LP, Hsieh CC, Chen LW. Macromolecules 1998; 31:1229–35.

[80] Bates WD, Shenoy SL, Wnek GE. In preparation.

[81] Bates WD. Unpublished results.

[82] McKee MG, Elkins CL, Long TE. Polymer 2004;45:8705–15.

Submitted to *Polymer*, April 2005

Correlation between "Electrospinnability" and Physical Gelation

Suresh L. Shenoy[a]*, William D. Bates[a] and Gary Wnek[§]

[a] Chemical Engineering, Virginia Commonwealth University
Richmond, VA 23284-3028

[§] Department of Chemical Engineering, Case Western Reserve University
Cleveland, OH

* Corresponding author: sshenoy@vcu.edu

Abstract

Fiber formation by electrospinning is investigated for polymer solutions capable of physical gelation. It is shown that close to the gelation threshold, the combination of thermoreversible junctions and chain entanglements help to stabilize the liquid jet and overcome capillary forces thus giving micro/nano fibers. The effect of cooling time and temperature besides polymer concentration and molecular weight is clearly demonstrated for polyvinyl alcohol/water and polyvinylchloride/THF solutions. Finally the relationship between solvent quality, chain entanglements and poly(vinyl chloride) fiber formation is unequivocally illustrated.

Introduction

In the past decade electrostatic processing has been routinely employed to obtain ultra-fine fibers[1-3]. The process consists of applying a high voltage to inject a charge into a polymer solution of adequate concentration. As the voltage is increased, the drop of liquid presented at the tip of the syringe is attracted to the ground electrode thereby forming a Taylor cone. Above a critical voltage, the electrical energy, a consequence of the injected charge overcomes the surface tension and a continuous jet of liquid is ejected from the Taylor cone towards the target electrode. Ultrafine fibers are deposited on the collector due to evaporation of solvent on route. This technique has been employed to numerous polymer solvent systems to obtain fiber diameters ranging from tens of nanometers to hundreds of microns. A vast majority of studies reported in the literature concentrate on the application of the electrospun fibers[4-9]. Thus, fundamental understanding of the electrospinning process is limited. Only recently has there been a concerted push to gain fundamental insights into the electrospinning process. For example a number of efforts have concentrated on modeling the whipping instability and predictions of fiber diameter [10-17]. However, there has been a lack of knowledge with regards to fiber formation and its relationship to the polymer solution properties. Recently, McKee et al. investigated the solution properties, in particular the viscosities of linear and branched polyesters, and proposed that fiber formation occurs at the entanglement concentration [18]. Over the past year we have particularly interested in the effect of polymer solution properties on fiber initiation/ fiber formation or "electrospinnability" (spinnability in electrostatic processing). In this regard we have demonstrated a clear link between chain entanglements in the solution and electrospinnability [19]. In particular we proposed a semi-empirical methodology to *a priori* predict the transition from electrospray to electrospin (or beads to fiber + beads) aptly named fiber initiation in good solvents. Additionally, we were also able to predict the transition from fiber + beads to solely fibers (complete fiber formation). The salient features of the approach are described below.

In the electrospinning process, while it is accepted that chain entanglements inhibit the jet breakup during acceleration to the target electrode, the relationship between fiber formation and polymer structure, molecular weight and concentration is only now being investigated. In order to facilitate predictions from spray to spin, as part of our model, we have defined the solution entanglement number $(n_e)_{soln}$ as the ratio of the polymer weight molecular weight (M_w) to the polymer entanglement molecular weight in solution, $(M_e)_{soln}$.

$$(n_e)_{soln} = \frac{M_W}{(M_e)_{soln}} = \frac{\varphi M_W}{M_e} \qquad (1)$$

Here, M_e is the entanglement molecular weight in the melt and ϕ is the polymer volume fraction. Note that M_e is generally a function of chain topology or geometry and ϕ accounts for the dilution effect due to presence of solvent. Using the results from polymer solution rheology, a correlation was established between initiation of fiber formation (spray to spin transition) and upturn in zero shear viscosity/M_w plot. Thus in terms of the entanglements, fiber formation is initiated at $(n_e)_{soln} = 2$ (or # of entanglements per chain =1). The veracity of this correlation was demonstrated by comparing the predicted polymer concentrations with experimental observations for a number of polymer/solvent systems. The applicability of this approach is clear since a wide range of systems were tested including those involving strong polymer-solvent hydrogen bonding (PEO/water and PVP/ethanol). Wilkes et al. have reported a similar approach where they employed the entanglement concentration obtained using viscosity data, to explain the spray to spin concentration for linear and branched polyesters. With the use of $(n_e)_{soln}$ (or # entanglement per chain) our approach allows *a priori* prediction of the appropriate concentration for good electrospinnability without having to measure solution viscosities.

Besides fiber initiation, it was demonstrated that the critical concentration for complete fiber formation (no beads or beaded fibers) corresponds to $(n_e)_{soln} = 3.5$ (average of 3-4) i.e. the number of entanglements per chain ~ 2.5 (average of 2-3). Based on the results of Schreiber et al.[20] and Hayahara et al.[21] for dry spinning, we believe this corresponds to the formation of an elastically deformable network under the influence of an elongational flow field. An advantage of this semi-empirical approach is that the only parameter required for the predictions is the melt entanglement molecular weight, M_e. Thus, for any given polymer, the spray to spin transition and complete fiber formation (electrospinnability) can be calculated for any concentration/molecular weight space. Note that an underlying assumption of our approach is that chain entanglements are solely responsible for the upturn in solution viscosity and the formation of the elastic network under the influence of an elongational strain. Thus the approach is valid only for the good solvent case where polymer-polymer interactions are negligible.

However, in systems where strong interactions such as hydrogen or ionic bonding are present, polymer-polymer interactions may not be negligible. Increased inter-chain interactions in these systems may serve to stabilize the physical (chain) entanglements by retarding chain disentanglement or forming additional junction points which may facilitate fiber formation at concentrations lower than predicted by equation 1. Other factors such as liquid-liquid (L-L) phase separation [22] into microdomains (microphase separation) in conjunction with vitrification and/or solid-liquid (S-L) phase separation (crystallization) can also serve a similar purpose by creating additional junction points thereby lowering the concentration threshold for fiber formation. In these systems, the upturn in solution viscosity could be due to the combination of various factors; namely chain entanglements, polymer-polymer interactions and phase separation (L-L, S-L).

In previous work from our laboratory, Kenawy et al.[22] have described a classical system where we believe both L-L and S-L phase separation assists fiber formation. Electrospun mats of ethylene vinyl alcohol copolymers containing 56-71 wt% vinyl alcohol were obtained by electrospinning from rubbing alcohol (70% 2-propanol/30% water, vol:vol). Due to copolymer crystallinity, application of heat (80°C) was a prerequisite to completely dissolve the copolymer. Upon cooling to room temperature, electrospinning results in EVOH fibers. However, polymer precipitation was

always observed, but not until several hours after cooling the solution to room temperature. Since precipitation of EVOH is kinetically quite slow, fiber formation was quite extensive prior to precipitation. Previously, we had speculated that the thermodynamic instability resulting from proximity to liquid-liquid phase separation (upper critical solution temperature or UCST) might be promoting the electrospinning process and subsequent fiber formation [23]. Of course, an additional driving force could be solid/liquid phase separation (crystallization) or a combination of the two (crystallization + UCST). The microscopic crystallites or 'embryonic nucleation sites' comprising of fringed micelles or chain folded crystals can easily serve as junction points where several different polymer chains, come together. The entanglement approach described in our most recent work is clearly not adequate for this type of system. In contrast to the dynamic nature of the physical entanglements i.e. entanglements formed by crossing over (or knotting), the crystallite junctions are essentially semi-permanent (dissolves at crystallite T_m). Clearly, a combination of the microcrystalline junctions with physical entanglements can facilitate fiber formation.

Additionally, in the course of electrospinning studies, we have frequently observed that the polymer solutions form physical gels quite unlike the precipitation observed for EVOH systems. For example, poly(vinylidene fluoride) (PVDF)/dimethyl formamide (DMF) solutions are prone to form physical gels on cooling to room temperature within a few hours, particularly at high polymer concentrations [24]. The solution can regain its fluidity upon reheating the PVDF/DMF gel. Another system which behaves in a similar manner is completely hydrolyzed (> 99%) poly(vinyl alcohol) (PVA)/water [25]. Both systems required application of heat to completely dissolve the semicrystalline polymers (PVDF, PVA). Upon cooling to room temperature the solutions undergo thermoreversible gelation, quite unlike EVOH, where precipitation of EVOH from 2-propanol/water solutions is observed. Interestingly despite the differences in the outcome of the final morphology of the solutions the mechanisms are quite similar. Thus, it is possible that mechanisms that promote physical gelation also aid in extensive fiber formation in these systems (PVDF, PVA). Clearly the chain entanglement picture is inadequate to explain fiber formation in these systems. In this paper, we attempt to investigate correlations between electrospinnability (fiber formation) and physical or thermoreversible gelation. Our interest in this topic is particularly fuelled by the vast amount of literature on physical gelation of synthetic and biopolymers thereby raising the possibility of obtaining electrospun mats from a number of biopolymers [26,27]. In this paper however, for the sake of simplicity we concentrate solely on synthetic polymers.

Physical Gelation of Polymer solutions

Physical gels are a 3-D network of chains in which the junction points are formed as a result of some type of molecular or chain association e.g. helix formation, complex formation or hydrogen bonding resulting in regions of local order [27]. The physical junctions can also arise through phase transitions such as liquid-liquid (L-L) or solid-liquid (S-L) segregation or a combination of the two (L-L + S-L) [27-30]. Consequently

both thermodynamics and kinetics play a vital role in the formation and the morphology of these physical gels. Therefore these systems can seldom be considered to be in strict thermodynamic equilibrium. For more details on various facets of gel formation, including mechanical and thermal properties and gel morphology, the reader is referred to a number of authoritative reviews/books [26,27].

Briefly, gelation is a function of polymer concentration, molecular weight, temperature, solvent quality and cooling (quench) rate. From an electrospinning perspective, network formation (due to physical junctions) during thermoreversible gelation is of particular interest. For any given solvent this process occurs over a temperature (T) or a concentration (ϕ) range. For example at a constant T, polymer chains in a dilute solution behave as isolated coils. As the concentration is increased above the overlap concentration (ϕ^*), intermolecular interactions (or embryonic nucleation of microcrystallites) can result in aggregation of several coils forming clusters. The dynamic behavior of polymer chains is now significantly influenced by the polymer-polymer interactions. Further increase in polymer concentration can enhance the size of these clusters as the surrounding free chains are trapped in these aggregates. This is accompanied by a concomitant increase in solution viscosity. Eventually at a critical concentration, a network is formed as polymer chains become entrapped in a number of these primary aggregates resulting in physical gelation. This process can be reversed simply by application of heat (or cooling in some cases) to eliminate intermolecular interactions (or dissolve microcrystallites) to obtain aggregate-free solutions. Note that based on the mechanism described above, solvent quality can be an important parameter. Thus choosing low affinity solvents would result in increased polymer-polymer interactions and consequently lead to higher chain aggregation and rapid gelation. For example, polymer/solvent systems which undergo L-L phase separation through spinodal decomposition result in the formation of a network type structure (due to nucleation and growth) when accompanied/followed/preceded by vitrification or crystallization [27-30]. However, while low solvent affinity is an important parameter, it is not a necessary condition for physical gelation to occur. Over the past decade, Guenet et al. [26,31,32] have clearly demonstrated that thermoreversible gels can also be obtained in good solvents and hence is not limited to poor solvents as previously believed.

Our interest in physical gelation was kindled when we realized that an appropriate choice of polymer concentration (ϕ) or temperature (T) would enable us to electrospin polymer solutions before the gelation process commenced. Note that this is different from the traditional gel spinning technique often employed to obtain fibers from PVA, cellulosic esters, acrylonitrile-vinyl chloride copolymers and ultra high molecular weight polyethylene (UHMWPE). Briefly gel spinning is intermediate between dry and wet spinning and consists of extrusion of a highly concentrated polymer solution or plasticized gel through spinnerettes. In the current situation the solution concentration is appropriately chosen so that physical gelation occurs on the outer surface of the ejected liquid jet as the solvent evaporates before capillary forces can break up the jet. It is here, that the presence of aggregates or clusters in the pregel solutions becomes critical. The parameters (ϕ, T) have to be chosen carefully so that the number of aggregates present in the solution is adequate to stabilize the ejected liquid jet (and aid fiber formation), but not so widespread that physical gelation commences in the syringe. However, obtaining information on the aggregates (number, size) is not a trivial task. Intuitively one can

expect that aggregation formation would become more prevalent and rapid as the solvent quality diminished. In addition to polymer/solvent thermodynamics, kinetics (slow versus fast cooling, time dependence) also plays a significant role. Thus, in contrast to jet stabilization by chain entanglements discussed previously, a priori prediction of fiber formation in solutions capable of physical gelation is a non-trivial task. Nevertheless, our aim in this paper is at the very least to present a few guidelines (e.g. ϕ, M_w) that can serve as a catalyst for future research in this area. These rules of thumb are empirically deduced by analyzing electrospinning results published in the literature or from experiments performed in our laboratory.

Prior to discussing and analyzing some polymer/solvent systems, we would like to recap some of the results on physical gelation. In general, the threshold concentration above which gelation occurs $[(\phi_{gel})_{threshold}]$ is > chain overlap concentration (ϕ^*). As ϕ is increased, increased chain overlap eventually leads to chain entanglements $((n_e)_{soln}-1)$. Thus usually in a physical gel one can expect two types of junctions to be present; a reversible or semi-permanent junction that can be eliminated by cooling or application of heat as described earlier and a dynamic one i.e. entanglement(s). However, note that presence of chain entanglements for physical gelation to occur is not a necessary condition as has been demonstrated by Boyer et al. [33]. Finally, thermoreversible gelation is not limited to poor solvents and can also occur in good solvents.

In exploring a relationship between fiber formation in electrospinning and physical gelation, we first consider a system where the presence of UCST + S-L phase separation is well known; namely poly(vinyl alcohol) (PVA)/water [25,34,35]. Additionally the effect of Mw and solvent quality on PVC electrospinning in three different solvents (good, marginal and poor) is explored, namely tetrahydrofuran (THF), morpholine (MOR) and dioxane (DOA).

PVA/water

Fabrication of electrospun PVA mats has been of particular interest to us due to PVA biocompatibility and potential use as a tissue-engineering scaffold. PVA is generally produced by saponification or hydrolysis of poly(vinyl esters), generally poly(vinyl acetate). Thus polymer properties (e.g. crystallinity, wettability) are a strong function of the degree of hydrolysis.{Pritchard, 1970 #169} In addition, tacticity is also an important parameter affecting PVA properties specially crystallinity {Pritchard, 1970 #169}. Electrospinning of PVA with degree of hydrolysis ranging from 87-96% is fairly straightforward. However as reported by Yao et al.[37] from our laboratory, fiber formation in a reproducible manner for fully hydrolyzed PVA (> 99%, M_w = 115k) was possible only upon the addition of a surfactant (Triton X-100). For a 10 wt% PVA in deionized water, the critical surfactant concentration for complete fiber formation was determined to be 0.3 % (w/v). It was concluded that the inability to electrospin fully hydrolyzed PVA was probably a combination of high surface tension of water and tendency of PVA to undergo gelation. It was suggested that addition of the surfactant probably retarded PVA gelation while lowering surface tension. More recently, Koski et

al. [38] established a correlation between [η]c value and electrospinning for PVA/water solutions. Unlike the results obtained in our lab, the authors were able to electrospin high M_w fully hydrolyzed samples. However, the quality of the fibers was poor and included a broad distribution of fibers and beaded fibers. In contrast to these results, Zeng et al. [39] reported complete fiber formation from PVA/water solutions for M_w as high as 195k without use of additives. Thus literature data appears to be inconsistent.

We attempt to investigate reasons for these discrepancies by correlating fiber formation and calculated solution entanglement number i.e. $(n_e)_{soln}$ (equation 1). If the entanglement analysis were applicable to the PVA/water solution [40-43], one would expect fiber initiation to occur for $(n_e)_{soln} \sim 2$ and complete fiber formation for $(n_e)_{soln} \geq 3.5$ (# entanglements/chain ≥ 2.5) [19]. Table 1 lists calculated $(n_e)_{soln}$ for all the systems considered in this paper. Clearly for PVA/water, there are inconsistencies in the calculated $(n_e)_{soln}$ values which correspond to complete fiber formation. For example, using the experimental observations of Koski et al.[38] the transition from fibers + beads to complete fiber formation occurs for $(n_e)_{soln} \geq 1$ (number of entanglements/chain ≥ 0). On the other hand, using Zeng's observations, the transition value is higher; $(n_e)_{soln} \geq 2$ (number of entanglements/chain ≥ 1 i.e. onset of entanglements). Of course both these values are lower than that predicted by the entanglement analysis [$(n_e)_{soln} \geq 3.5$] for complete fiber formation [19]. We believe both the differences in the ability to electrospin high M_w PVA (Yao et al.[37], Koski et al.[38] and Zeng et al.[39]) and lower $(n_e)_{soln}$ values corresponding to fiber formation are related to the propensity of PVA solutions to undergo physical gelation. We attempt to address each issue separately.

One of the mechanisms necessary for fiber formation in conventional and electrostatic spinning is the presence of stabilizing junctions such as those provided by chain entanglements. Under the action of an elongational stress, an elastic network is created thereby stabilizing the jet flow against capillary effects. In solutions susceptible to physical gelation, we believe that the thermoreversible junctions (responsible for gelation) in conjunction with chain entanglements are responsible for stabilization of the ejected liquid jet from the Taylor cone and consequently fiber formation. From the point of view of obtaining an elastic deformable network (necessary for fiber formation), the thermoreversible junctions (responsible for gelation) are considered to be purely elastic, since in a mechanical test they generally exhibit reversible deformation after a short relaxation. For PVA/water solutions, these thermoreversible junctions are probably "microcrystallites" formed in solution (S-L phase separation) or a combination of spinodal decomposition (L-L phase separation) together with formation of microcrystallites upon cooling. Each microcrystallite junction is made up of different chains thereby linking different crystallites and forming a network. Prins et al. [34,35] and Komatsu et al. [44] have given more details on the mechanism including the phase diagram to describe PVA gelation. Using the phase diagrams, it appears that PVA fiber formation corresponds to region where sol → gel (see Figure 5 in Komatsu et al.[44]). For the PVA/water system, the transition from sol to gel is slow (hours) while solutions are generally electrospun immediately after cooling the hot PVA solutions to room temperature. This of course makes it a time dependent process. Therefore, we can expect electrospinning solutions to have some aggregates (due to thermoreversible junctions) but not nearly enough for physical gelation. These aggregates act as additionally stabilizing factors and hence $(n_e)_{soln}$ (see Table 1) corresponding to jet stabilization against capillary

forces and fiber formation would be lower than previously predicted (3.5 [19]). Note that in reality, formation of microcrystalline junctions is a complex process and dependent on the stereo-regularity of PVA, degree of hydrolysis and thermal history.

Another issue of importance are the differences in the calculated value of $(n_e)_{soln}$ corresponding to complete fiber formation for high M_w PVA (Table 1). We believe these differences are related to the thermal history of the solutions. It is well known that homogenous PVA solutions are formed at high temperatures ($\geq$ 80°C) and undergo gelation upon cooling. The gelation temperature is a strong function of the cooling rate and reproducibility is observed only when the cooling rate is < 1°C/hr. Additionally, time is an important parameter affecting the number of aggregates (thermoreversible junctions) present in the solution. While both Yao et al.[37] and Koski et al.[38] heated PVA solutions to 80°C, in the case of Yao et al., the solution was cooled to room temperature prior to electrospinning. On the other hand, Koski et al. electrospun PVA immediately after the PVA had dissolved. No information has been provided about the electrospinning solution temperature. It is entirely possible the cooling time and hence electrospinning temperature are different in the two cases (Yao et al. and Koski et al.) resulting in differences in the number and size of supramolecular aggregates. The presence of large number of these supramolecular aggregates in the cooled solutions of Yao et al. could result in microgel formation and hence electrospraying of large blobs. On the other hand, Zeng et al.[39] heated the PVA solution to 95°C for a period of > 3 hrs to aid dissolution. No mention has been made of the electrospinning solution temperature. Fibers with diameters ranging from 350 nm-700 nm were obtained upon electrospinning an 8 wt% solution of 195k PVA. Zeng's observations suggest that the transition from fiber + beads to fibers is predicted to occur at $(n_e)_{soln} \geq 2$. We think the reason for the discrepancies between calculated $(n_e)_{soln}$ values corresponding to fiber formation is the PVA dissolution temperature. Previous studies on PVA solutions indicate that a temperature of at least 92°C is needed to completely dissolve PVA [27]. Thus at 80°C, many microcrystallites (thermoreversible junctions) may be still present. Therefore for a dissolution temperature of 95°C, formation of the supramolecular aggregates is slower since crystalline nuclei have been eliminated during the heating process. Therefore a higher number of chain entanglements would be required [$(n_e)_{soln} \geq 2$] to compensate for the lower number of aggregates to stabilize the liquid jet. The same cannot be said for solutions heated to 80°C.

Another factor not mentioned so far is the effect of M_w. It is well known that in general possibility of network formation (and hence gelation) is greater as polymer M_w increases. This is evident from the fact that the gelation temperature increases (or cooling time increases) as M_w increases. Thus, especially in solutions heated to 80°C one would expect to see a strong M_w effect. For the higher M_w polymer (115k), the aggregate formation is much faster and hence by the time the solution is electrospun, gel-like blobs like those reported by Yao et al. are obtained instead of fibers. For the lower M_w polymer, the network formation is just sufficient to allow fiber formation to occur (but not physical gelation) as has been observed by Koski et al. Heating the high M_w solution to 95°C eliminates the crystal nuclei thereby slowing down the aggregate formation process and allowing fiber formation on cooling.

To check this hypothesis, we electrospun PVA solutions (same polymer sample used by Yao et al.; M_w = 115k)[37] of different concentrations (6, 8 and 10 wt%) by

heating to 95°C (instead of 80°C) for about 12 hrs [45]. Figure 1 (a-c) (results tabulated in Table 1) shows optical micrographs of the morphologies obtained upon electrospinning PVA solutions. Note that electrospinning was carried out immediately upon cooling to room temperature. It is clear that complete fiber formation is observed at 10 wt%. The calculated $(n_e)_{soln}$ value corresponding to complete fiber formation also appears to correlate with the onset of entanglements i.e. $(n_e)_{soln} = 2$, in good agreement with values calculated using the experimental observations of Zeng et al. [39]. These findings are in contrast to previously published results [37] discussed in earlier paragraphs when solutions were heated to 80°C. Furthermore, as PVA concentration is reduced from 10 wt%, beads and beaded fibers are observed, as one would expect. We have also investigated the effect of time. Figures 1d-f shows optical micrographs of electrospinning solutions (6-10 wt%) 45 minutes after the solution has cooled from 95°C to room temperature. For the 10 wt% solution, as time elapses, development of aggregates (significant thermoreversible junctions) prevents fiber formation even at 30 kV due to a drastic increase in viscosity. For 8 wt%, gel-like blobs interspersed with a few fibers are obtained. This indicates that for the 8 wt% solution, a sol-gel type separation of the solution occurs probably due to continued aggregate formation. This type of separation is limited for the 6 wt% solution due to lower PVA concentration. Fiber formation is therefore a function of time in addition to ϕ and M_w. This time-dependent phenomenon or ageing has been previously discussed in the thermoreversible gelation literature [27]. Thus for PVA solutions, the optimum number of entanglements/chain necessary for fiber formation is a function of M_w, thermal history, time and the temperature of electrospinning. We are currently in the process of evaluating effects of ϕ, M_w and time at various temperatures on fiber formation in solutions capable of gelation and detailed results will be forthcoming in a future publication.

Finally we conclude this section by considering PVA fiber formation data reported by Koski et al.[38] for the lowest molecular weight (M_w = 9-10k). The calculated $(n_e)_{soln}$ values corresponding to fiber formation are < 1 i.e., fiber formation occurs in the absence of chain entanglements. We believe a possible explanation for this deviation is higher crystallinity and the effect of functional end groups in lower molecular weight samples. Sato et al.[46] have meticulously investigated the effect of both M_w and chain end groups on physical properties of PVA. The authors concluded that crystallinity increased as M_w decreased irrespective of the chain end functionality. On the other hand, physical properties such as swelling of PVA films in water were observed to be a strong function of end group functionality. It is plausible that both higher crystallinity and interactions between chain end groups (for example; carboxylate groups) can result in stabilization of the jet at significantly lower concentrations than anticipated $[(n_e)_{soln} < 1]$. This hypothesis needs to be confirmed by electrospinning at higher temperatures and by using non-interacting functional end groups.

Poly(vinyl chloride) (PVC)

PVC is a polar polymer where the tacticity has a significant influence on the resulting polymer crystallinity quite similar to PVA. Lee et al.[47] explored PVC fiber formation by electrospinning as part of a study investigating the effect of mixed solvents. Briefly, Lee et al. concluded that, while pure THF did not facilitate electrospinning of PVC (degree of polymerization = 800) due to repeated blockage of the syringe tip, certain solvent ratios of THF/DMF did facilitate fiber formation. In addition, Gupta et al.[48] demonstrated the possibility of side-by-side bi-component electrospinning using PVC and PVDF.

Our initial interest in PVC was to explore the role of chain entanglements versus the propensity to undergo physical gelation on fiber formation. As a result we investigated the effect of both M_w and solvent quality on PVC fiber formation. Table 3 lists the molecular weight (M_w) of the PVC samples employed for electrospinning. Preliminary experiments indicate that fiber formation (defect free, no beads or beaded fibers) from THF is inconsistent. This problem is particularly acute for the highest M_w sample as shown in Figure 2a. However upon heating the solutions to ~ 70°C, fiber formation from THF is in fact quite extensive (see Figure 2b). This observation is analogous to PVA electrospinning described in earlier sections. The key difference is that while THF is a good solvent for PVC, the PVA/water solutions undergo both L-L and S-L phase separation upon cooling. Another interesting observation is the reduction in molecular weight (specially for the highest M_w sample) upon application of heat to PVC/THF solution. This result might explain the difficulty in electrospinning high PVC solutions (specially high M_w) prior to heating. Gel Permeation Chromatography given in Table 3 shows that for the highest molecular weight sample, M_w decreases from 343k to 249k after heat treatment. The M_w appears to increase again, to 260k according to the measurement 96 hours after heat treatment. At present we are not sure if this is simply within the limits of error of the instrument or if it is a genuine trend since we have not investigated M_w as a function of time for $t > 96$ hrs. Based on published reports [26,27,49,50], we believe aggregation of syndiotactic sequences in PVC is responsible for the apparent higher M_w prior to heating. The aggregration is extensive enough to prevent consistent defect-free fiber formation. Application of heat destroys the aggregates, which lowers M_w and also promotes fiber formation [27]. This hypothesis is also validated by published light scattering and NMR spectroscopy data on pregel PVC solutions [26,27]. We believe this phenomenon is restricted to the high M_w sample since the reaction methodology employed to obtain high M_w PVC (traditionally low reaction temperature) also results in an increase in the number of the syndiotactic sequences consequently increasing aggregration [27]. While the change in M_w on heating is negligible for the 90k and 210k samples, the issue of inconsistent fiber formation nevertheless remains true. It is possible that for these samples aggregration is very subtle at the solutions concentrations employed for GPC measurements (0.6 wt%). On the other hand significantly higher concentrations are required for PVC fiber formation (by electrospinning 10-16 wt% depending on the M_w), which results in considerable levels of aggregration, and hence inconsistent fiber formation.

For the sake of consistency for all calculation we have employed the M_w obtained in our laboratory by GPC after heating the solutions. Using $(M_e)_{PVC} = 4310$ gm/gmol [41-43,51] in the entanglement analysis i.e. equation (1), it is predicted that for the 210k sample, fiber initiation (mixture of beads + fibers) should commence around 6.4 wt%

($(n_e)_{soln}$ = 2) and only fibers should be obtained for concentrations ≥ 10.8 wt% ($(n_e)_{soln}$ = 3.5). Figure 3 shows the optical micrographs of the PVC morphologies obtained by electrospinning solutions of different concentrations from THF. Fiber initiation occurs ~7 wt% and for 11 wt% only fibers are obtained thus validating our predictions. However, for solutions with higher PVC concentration (12 wt%), high solution viscosity inhibits extensive fiber formation. Eventually 14 wt% PVC solution undergoes a partial sol to gel transition in approximately 72 hrs. On the other hand, for the 11 wt% solution no gelation was observed even after a week. The observation of PVC gelation in THF came as a surprise to us. While there appears to be a wealth of information on PVC gelation in a variety of solvents [26,27], gel formation in THF, a good solvent has not been reported, though it is a distinct possibility given the results of Guenet et al.[31,32] What is unclear and not the subject of our study is the PVC gelation mechanism in good solvents such as THF (as opposed to poor solvents), i.e. microcrystallites or polymer-solvent compounds. Irrespective of the gelation mechanism, our interest lies in the determining correlations between PVC gelation in good solvents such as THF and fiber formation.

Effect of MW on mechanism of jet stabilization

To do this, we investigated the effect of PVC M_w on electrospinning [52]. Table 2 presents the results for M_w = 343k, 251k and 108k. The true M_w for these samples obtained by GPC correspond to 249k, 210 and 91k respectively. Note that the true M_w's are used in equation 1 to calculate $(n_e)_{soln}$ corresponding to fiber formation. For the higher M_w (true) sample i.e. 249k, the entanglement analysis predicts that the transition from beads to fibers + beads should occur around 5.5 wt% and only fibers should be obtained for concentrations ≥ 9.5 wt%. The experimental results reported in Table 1 for the 249k PVC are in good agreement with the predictions. For the lower M_w solutions (91k), assuming no gelation, the corresponding transitions are predicted to be ~14.2 wt% and 23.7 wt%. Surprisingly, as shown in Figure 4, fiber initiation occurs ~10 wt% and complete fiber formation (no beads or beaded fibers) is observed around 16 wt%. For the lower molecular weight (91k) PVC, reconciling the experimental observations with the entanglement analysis (equation 1, [19]) is difficult. Based on arguments made for PVA/water solutions, it is plausible that for the 91 k sample chain entanglement may not be the sole mechanism for formation of elastic network and hence fiber formation. This hypothesis is validated by the fact that for a 18 wt% solution, gelation occurs within 3-4 hrs. Interestingly, the calculated $(n_e)_{soln}$ values corresponding to complete fiber formation (M_w = 91 k) is ~ 2, signifying the presence of 1 entanglement/chain. Thus supramolecular aggregates (due to thermoreversible junctions) in the lower M_w PVC solutions play a vital role in fiber formation.

However an obvious question remains unanswered. Upon decreasing M_w from 249k, at what point does the mechanism for fiber formation change from simply physical entanglements to a combination of entanglements and thermoreversible junctions

(corresponding to gelation)? We believe the answer lies in probing M_w dependence of $(\phi_{gel})_{threshold}$ and $(\phi_{el})_{fiber}$ where $(\phi_{gel})_{threshold}$ is the threshold concentration (volume fraction) at which gelation occurs and $(\phi_{el})_{fiber}$ is the concentration (volume fraction) at which an elastic network is obtained giving only fibers . Decreasing M_w increases both the $(\phi_{gel})_{threshold}$ and $(\phi_{el})_{fiber}$. From a theoretical perspective, previous studies on atactic polystyrene (aPS) gelation in poor solvents have suggested that [33,53]

$$(\phi_{gel})_{threshold} \alpha (M_w)^{-0.5} \quad (2)$$

On the other hand, for PVC/THF solutions, equation (1) can be rewritten as

$$(\varphi_{el})_{fiber} = \left(\frac{3.5M_e}{M_w}\right) = \frac{15085}{M_w} \quad (3)$$

which implies that $(\phi_{el})_{fiber} \alpha (M_w)^{-1}$. Thus the M_w dependence of $(\phi_{gel})_{threshold}$ is weaker.

Figure 5 compares both the theoretical and the experimental observed values for $(\phi_{gel})_{threshold}$ and $(\phi_{el})_{fiber}$ for the different molecular weight PVC solutions. The experimental values of $(\phi_{gel})_{threshold}$ for all samples was assumed to the polymer volume fraction in solution which results in gelation in approximately 6 hrs. Though this time frame is completely arbitrary, it still allows us to show that the transition from a purely entanglement mechanism to combination of entanglement and gelation is due to the weak M_w dependence of $(\phi_{gel})_{threshold}$. Obtaining the experimental $(\phi_{el})_{fiber}$ is fairly straightforward and consists of determining the concentration by electrospinning PVC/THF solutions of the different M_w's.

To obtain theoretical $(\phi_{gel})_{threshold}$ we have employed $(\phi_{gel})_{threshold}$ determined experimentally for the 91k sample as the reference i. e. $(\phi_{gel})_{threshold\ 91} = 0.125$ vol % (0.18 wt fraction). Then theoretical $(\phi_{gel})_{threshold}$ for any molecular weight samples is calculated using equation 4

$$(\varphi_{gel})_{threshold\ Mw} = (\varphi_{gel})_{threshold\ 91}\left(\frac{M_{w91}}{M_w}\right)^{0.5} \quad (4)$$

which is derived from equation 2. For the current samples, M_w will be 210k and 249k respectively. For $(\phi_{el})_{fiber}$, the theoretical curve is obtained using equation 3. Note that this specific curve is valid for PVC/THS solutions only since it involve $(M_e)_{PVC}$.

Figure 5 clearly shows that for $(\phi_{el})_{fiber}$ there is excellent agreement between theory and experiment for the higher Mw's (210k and 249k). However for the lower Mw the experimental value is considerably lower than predictions (0.11 versus 0.176). For $(\phi_{gel})_{threshold}$, the experimental value appears to higher than the theoretical predictions (0.11 versus 0.082 for 210k and 0.095 versus 0.076 for 249k). Clearly the experimental Mw dependence of $(\phi_{gel})_{threshold}$ is weaker than predicted by equation 2. This maybe ascribed to the differences in the gelation mechanism. Note that equation 2 was deduced theoretically for aPS. Gelation of aPS has been attributed to a combination of L-L phase separation and vitrification [28,29,33]. In contrast, PVC/THF gelation is clearly a result

of S-L phase separation (microcrystallites) or polymer-solvent compounds [26,27,31,54]. Thus strictly speaking equation (2) is not valid for PVC/THF. In fact we expect $(\phi_{gel})_{threshold}$ to be weaker function of M_w (than eqn 2) since the effect of chain length on polymer crystallization is insignificant for the lengths under consideration (91k to 249k). Our experimental observations (given in Table 4) for $(\phi_{gel})_{threshold}$ clearly validate this hypothesis.

In Figure 5 we clearly notice a crossover of the $(\phi_{gel})_{threshold}$ and $(\phi_{el})_{fiber}$ curves at approximately 155k gm/mol, $(M_w)_{crossover}$. For PVC samples with $(M_w)_{crossover} > 155k$, as one increases the PVC concentration (depicted as line A in Figure 5), its is clear that $(\phi_{el})_{fiber}$ is attained prior to $(\phi_{gel})_{threshold}$. Thus we can conclude that for the 249k and the 210k solutions, fiber formation at concentrations corresponding to fiber formation i.e. ~9 wt% ($\phi = 0.06$) and 11wt% ($\phi = 0.074$) respectively is primarily due to stabilization by chain entanglements. Our hypothesis is validated by the light scattering results of Hong et al.[55] who found no evidence of aggregrates for a 6 wt% 500k PVC/THF solutions. In contrast for $M_w < (M_w)_{crossover}$, upon increasing PVC concentration (line B in Figure 5), one encounters $(\phi_{gel})_{threshold}$ is attained prior to $(\phi_{el})_{fiber}$. Thus we can conclude that for the 91k sample, thermoreversible junctions in conjunction with chain entanglements (since $(n_e)_{soln} \geq 2$ or number of entanglements ≥ 1) are responsible for jet stabilization. Note that this type of analysis (equation 3) for good solvents with negligible polymer-polymer specific interactions.

Effect of solvent quality on PVC electrospinning

From the discussion so far, it is clear that fiber formation in electrospinning is strongly influenced by the propensity of the polymer solution to gel. This implies that solvent quality significantly affects gelation and consequently fiber formation during electrospinning. For example, it has been suggested that crystallinity in PVC gels is a function of the polymer-solvent interactions.[26,27] Similar results have been reported for PVA gels.[56] More recently Hong et al.[55] have extensively investigated the effect of solvent quality on the PVC (M_w = 500k) gelation behavior. Three solvents having similar molar volumes and functional groups but dissimilar charge density arrangements and hence dipole moments; namely tetrahydrofuran (THF), morpholine (MOR) and dioxane (DOA) were employed. The results relevant to our work are briefly summarized;

(i) The strength of the polymer-solvent interactions was established to be PVC/THF > PVC/MOR > PVC/DOA. In addition, by extrapolating the second virial coefficient to zero i.e. A_2=0, the θ-temperatures for PVC/THF, PVC/MOR and PVC/DOA were determined to be approximately 0, 56 and 70°C respectively.

(ii) Formation of aggregates in the solution was demonstrated to be a function of solvent quality; i.e DOA > MOR. No aggregation not observed in THF even at the largest concentrations (6 wt%) employed in the study.

(iii) Not surprisingly the ease of gelation was determined to be a function of solvent quality, namely; DOA>MOR. The gelation concentration threshold

was measured to be about 2.2 wt% in DOA and about 4 wt% in MOR. No gelation was observed in PVC/THF solutions at 6 wt%.

(iv) Gelation mechanism in MOR and DOA was speculated to be the result of both L-L and S-L phase separations.

From our perspective, this in-depth investigation by Hong et al.[55] offers a unique opportunity to investigate the effect of solvent quality on PVC electrospinning. Note that despite the lower molecular weights used in our study, we expect the trends described above (i-iv) to also be valid for our samples.

PVC/MOR (M_w = 249k, 210k, 91k) and PVC/DOA (M_w = 210k) solutions were electrospun at various concentrations. The details of the experiments are given in the references [52]. During the course of our experiments we observed that the 7 wt% PVC/MOR and 4 wt% PVC/DOA (both 210k) solutions undergo rapid gelation upon cooling. On the other hand, lowering polymer concentration could allow us enough time to attempt electrospinning by retarding onset of gelation. Accordingly, Figures 5 and 6 show the optical micrographs of the morphologies obtained by electrospinning PVC/MOR (210k) solutions with concentrations ranging from 4-6 wt%. For the 4 wt% PVC/MOR solution (Figure 6), electrospinning of solution upon cooling clearly yields fibers with beads (Figure 6a). In addition, large blobs are also observed indicating presence of pregel aggregates or clusters in the solution. In contrast, electrospinning of the same solution 48 hrs after cooling to room temperature, yields large blobs/particles and no fibers as shown in Figure 6b. Additionally formation of a steady jet is not observed. The syringe tip appears to spit gigantic gel like blobs towards the target upon application of the voltage. This time dependent behavior is clearly a sign of onset of sol to gel transition. Figure 6 shows the morphology obtained by electrospinning 5 and 6 wt% PVC/MOR solutions immediately upon cooling. The micrographs 7a and 7b clearly demonstrate that for these concentrations an elastic deformable network is formed thereby supporting fiber formation. After 24 hrs, microgel formation is evident for the 5 wt% solution based on the presence of blobs in Figure 7c, while the 6 wt% solution completely undergoes gelation (Figure 7d) and cannot be electrospun.

For the PVC/DOA solutions, the PVC concentrations had to be reduced to avoid rapid gelation upon cooling, in good agreement with the results of Hong et al. (conclusion ii above). Figure 8 shows the optical micrographs of 1 wt% and 3 wt% PVC/DOA solutions electrospun at conditions identical to PVC/THF and PVC/MOR. At 1 wt%, only beads are observed. On the other hand spindle shaped beads are observed at 3 wt%. Electrospinning of the 4 wt% solution was not possible since it underwent rapid gelation on cooling to room temperature. Clearly while we are close to the transition for fiber initiation, the rapidity of physical gelation limits our ability to electrospin solutions of PVC/DOA where fiber formation maybe a possibility.

The higher and lower M_w PVC (249 and 91 k) was also employed to check effect on PVC fiber formation in MOR. The results are listed in Table 2. As expected, for the 91k PVC, fiber formation is extensive at higher polymer concentrations; i.e., 7 wt% instead of 5 wt% for the 210k sample. At concentrations > 9 wt% (versus 7 wt% for 210k), the solution undergoes gelation rapidly resulting in an unstable liquid jet. For the higher M_w solution i.e. 249k, fiber formation is observed at 4 wt% while gelation occurs rapidly at higher PVC concentrations.

In summary, the critical concentration above which fibers are obtained is a function of both; solvent quality (THF>MOR>DOA) and M_w. For PVC/MOR the critical concentrations are lower than in THF, namely 4 wt% versus 9 wt% for the 249k sample, 5 wt% versus 11 wt% for the 210k sample and 7 wt% versus 16 wt% for the 91k sample. On the other hand PVC fiber formation from dioxane (DOA) solutions was not possible due to the tendency to gel rapidly. These results are in very good agreement with the solvent quality trend determined by Hong et al.; namely (THF > MOR > DOA) [55]. For the 249k and the 210k sample in THF, we believe that formation of elastic network is probably a result of chain entanglements since $(n_e)_{soln} \sim 3.5$, while for the 91k sample fiber formation is due to a combination of chain entanglements and aggregrate formation since ($(n_e)_{soln} \geq 2$). In MOR (both 210k and 91k), it appears that while fiber formation is also due to a combination of pregel aggregates and chain entanglements. One can directly correlate this to the tendency for physical gelation due to L-L and S-L phase behavior. However in MOR fiber formation is obtained for $(n_e)_{soln} \geq 1$. These results are in contrast to the calculated $(n_e)_{soln}$ values (≥ 2) obtained for PVC/THF solutions corresponding to complete fiber formation. We believe that this due to the lower solvent quality of MOR than THF. Interestingly it also suggests that in THF the contributuion from chain entanglement and thermoreversible junctions maybe almost equal. However in MOR (a marginal solvent), almost all the stabilization is primarily due to the presenc of thermoreversible junctions ($(n_e)_{soln} \geq 1$ or number of chain entanglements ≥ 0 or minimal). For the 3 wt% PVC/DOA (91k) solution, $(n_e)_{soln} < 1$ indicating we are below the entanglement regime and thus it is no surprise that fiber formation is inhibited. The light scattering results of Hong et al. support our assertions. At room temperature, both MOR and DOA are poor solvents while THF is a good solvent. Thus aggregation in MOR and DOA prior to electrospinning is much more extensive than in THF. The consequence could be lower $(n_e)_{soln}$ values in poor solvents.

Final Thoughts

It is clear from our results (and conventional fiber spinning) that there is no single mechanism describing fiber formation in electrospinning. Essentially the ejected liquid jet has to be stabilized against capillary effects just long enough for solidification to occur principally through solvent evaporation. For wet electrospinning, the solidification will be a result of the coagulation of the outer layer of the liquid jet (similar to wet spinning). In the previous paper we looked at the systems where chain entanglements were the sole reason of jet stabilization. This mechanism appears to be limited to the good solvent case and where polymer-polymer interactions are negligible. In this paper we have identified yet another probable mechanism of jet stabilization. In polymers, which can undergo gelation even in good solvents, thermoreversible junctions in conjunction with chain entanglements provide stabilization long enough for fiber formation. However as seen from the M_w study (PVC/THF), this may be restricted for lower M_w polymers. This is primarily because of the unequal dependence of $(\phi_{el})_{fiber}$ and $(\phi_{gel})_{threshold}$ with M_w

(equations 2 and 3). For PVC equation 3 can be written in an exact form using equation 1 and the entanglement molecular weight (4310 gm/gmol) as

$$(\varphi_{el})_{fiber} = \left(\frac{3.5M_e}{M_w}\right) = \frac{15085}{M_w} \qquad (5)$$

Figure 8 shows the plot of $(\phi_{el})_{fiber}$ and $(\phi_{gel})_{threshold}$ with M_w. Both parameters increase with reduction of M_w. The intersection of the two curves gives us the critical M_w below which gelation becomes important. In other words below this M_w, both chain entanglements and thermoreversible junctions contribute to jet stabilization ($(n_e)_{soln} \geq 2$). Above this M_w, only chain entanglements are important and fiber formation can be predicted apriori using equation 1. For PVC, this critical value is 175k. Note that since we have previously established that equation 4 overestimates $(\phi_{gel})_{threshold}$ (due to differences in gelation mechanism), the value of 175k is an approximate value. Additionally this is valid for only for PVC in good solvents. However similar plots can be (e.g. PVA/water) plotted using the corresponding M_e values and determining the gelation threshold (equation 4).

Finally solvent quality is another important parameter that has been investigated in this paper. Our analysis shows that as solvent quality decreases, the mechanism for jet stabilization shifts more towards dominance of thermoreversible junctions. For example MOR is a marginal solvent for PVC. The calculated value of $(n_e)_{soln}$ corresponding to fiber formation is ≥ 1. Thus physical entanglements are present; they are secondary to the thermoreversible junctions. Another advantage of using a marginal solvent is that the polymer concentration corresponding to fiber formation is considerably less than for a good solvent. For a poor solvent like DOA, physical gelation is extremely rapid. Thus for concentrations where physical entanglements are present, gelation is too rapid for electrospinning to be attempted. At lower concentrations, electrospinning yields spindle shaped beads. This may be due to lack of any chain entanglements; $(n_e)_{soln} < 1$. Note that all our electrospinning experiments were performed at room temperature. Since gelation (aggregation) is affected by temperature, it is logical to reason that electrospinning at higher temperatures light offer unique opportunities for systems which undergo gelation at room temperature.

Conclusions

In this paper we have shown that fiber formation by electrospinning for solutions capable of physical gelation is possible. The conclusions of the investigation are summarized below;

(a) Fiber formation from PVA/water solutions is clearly a function of the dissolution temperature. Defect free fibers from high M_w PVA are obtained only when the dissolution temperatures is high enough (>92°C) to ensure elimination of embryonic crystallites.

(b) The contribution from chain entanglements i.e. $(n_e)_{soln}$ is a function of the dissolution temperatures. For lower temperatures i.e. 80°C, fiber formations corresponds to $(n_e)_{soln} \geq 1$ indicating the absence of chain entanglements. The thermoreversible junctions are solely responsible for stabilizing the liquid jet. In contrast for dissolution temperatures ≥ 92°C, fiber formation corresponds to $(n_e)_{soln} \geq 2$. Thus the liquid jet is stabilized by a combination of chain entanglements and thermoreversible junctions.

(c) In addition to the dissolution temperatures the elapsed time is another important factor, which influences fiber morphology.

(d) The fiber formation mechanism for PVC in a good solvent (THF) is a balance between the M_w dependence of the gelation concentration i.e. $(\phi_{gel})_{threshold}$ and the concentration corresponding to fiber formation due to chain entanglements only i.e. $(\phi_{el})_{fiber}$. For higher M_w (249 and 210k) PVC, $(\phi_{el})_{fiber}$ or chain entanglements dominate while at the lower Mw (91k) the liquid jet during electrospinning is stabilized by both chain entanglements and thermoreversible junctions.

(e) Besides M_w, solvent quality plays a vital role in determining the chain entanglement contribution. For marginal solvents such as morpholine, at low concentrations where no chain entanglements are expected, the significant number of thermoreversible junctions help to stabilize the jet and form fibers. Thus for PVC/MOR fiber formation is observed for $(n_e)_{soln} \geq 1$. Time is a important parameters for such systems. Longer cooling times results in abundance of the thermoreversible junctions, which increases viscosity dramatically preventing fiber formation.

(f) On the other hand if the solvent quality is poor such as with dioxane, gelation is rapid due to increased polymer aggregation and hence fiber formation is not observed.

(g) For solutions capable of physical gelation, fiber formation is thus a function of polymer concentration, M_w, temperature, solvent quality and cooling time

Acknowledgements

The authors would like to thank PolyOne for kindly donating sample of Geon 407. In addition the authors wish to thank Mr. Umit Makal at VCU, Chemical Engineering for GPC measurements. The authors would also like to thank DARPA (Bio-Optic Synthetic Systems Program) and the NASA Office of Space Sciences for generous support.

References

[1] Li D, Xia YN. Advanced Materials 2004; 16: 1151-1170.
[2] Huang ZM, Zhang YZ, Kotaki M, Ramakrishna S. Composites Science and Technology 2003; 63: 2223-2253.
[3] Frenot A, Chronakis IS. Current Opinion in Colloid & Interface Science 2003; 8: 64-75.
[4] Kenawy ER, Bowlin GL, Mansfield K, Layman J, Simpson DG, Sanders EH, Wnek GE. Journal of Controlled Release 2002; 81: 57-64.
[5] Matthews JA, Boland ED, Wnek GE, Simpson DG, Bowlin GL. Journal of Bioactive and Compatible Polymers 2003; 18: 125-134.
[6] Li WJ, Laurencin CT, Caterson EJ, Tuan RS, Ko FK. Journal of Biomedical Materials Research 2002; 60: 613-621.
[7] Schreuder-Gibson H, Gibson P, Senecal K, Sennett M, Walker J, Yeomans W, Ziegler D, Tsai PP. Journal of Advanced Materials 2002; 34: 44-55.
[8] Wang XY, Drew C, Lee SH, Senecal KJ, Kumar J, Samuelson LA. Journal of Macromolecular Science-Pure and Applied Chemistry 2002; A39: 1251-1258.
[9] Zussman E, Yarin AL, Weihs D. Experiments in Fluids 2002; 33: 315-320.
[10] Yarin AL, Koombhongse S, Reneker DH. Journal of Applied Physics 2001; 89: 3018-3026.
[11] Yarin AL, Koombhongse S, Reneker DH. Journal of Applied Physics 2001; 90: 4836-4846.
[12] Shin YM, Hohman MM, Brenner MP, Rutledge GC. Applied Physics Letters 2001; 78: 1149-1151.
[13] Shin YM, Hohman MM, Brenner MP, Rutledge GC. Polymer 2001; 42: 9955-9967.
[14] Spivak AF, Dzenis YA, Reneker DH. Mechanics Research Communications 2000; 27: 37-42.
[15] Fridrikh SV, Yu JH, Brenner MP, Rutledge GC. Physical Review Letters 2003; 90
[16] Feng JJ. Journal of Non-Newtonian Fluid Mechanics 2003; 116: 55-70.
[17] Feng JJ. Physics of Fluids 2002; 14: 3912-3926.
[18] McKee MG, Wilkes GL, Colby RH, Long TE. Macromolecules 2004; 37: 1760-1767.
[19] Shenoy SL FH, Bates WD, Wnek GE. Polymer 2004; submitted
[20] Schreiber HP, Rudin A, Bagley EB. Journal of Applied Polymer Science 1965; 9: 887-92.
[21] Hayahara T, Takao S. Journal of Applied Polymer Science 1967; 11: 735-46.
[22] Kenawy ER, Layman JM, Watkins JR, Bowlin GL, Matthews JA, Simpson DG, Wnek GE. Biomaterials 2003; 24: 907-913.
[23] Young TH, Cheng LP, Hsieh CC, Chen LW. Macromolecules 1998; 31: 1229-1235.
[24] Bates WD, Barnes CP, Ounaies Z, Wnek GE. Polymer Preprints 2003; 44: 114.
[25] Kawanishi K, Komatsu M, Inoue T. Polymer 1987; 28: 980-4.
[26] Guenet JM. Thermoreversible Gelation of Polymers and Biopolymers San Diego: Academic Press Inc., 1992.

[27] te Nijenhuis K, Editor. Thermoreversible Networks: Viscoelastic Properties and Structure of Gels, 1997.
[28] Tan HM, Chang BH, Baer E, Hiltner A. European Polymer Journal 1983; 19: 1021-5.
[29] Tan H, Moet A, Hiltner A, Baer E. Macromolecules 1983; 16: 28-34.
[30] Wellinghoff S, Shaw J, Baer E. Macromolecules 1979; 12: 932-9.
[31] Guenet J-M. Trends in Polymer Science (Cambridge, United Kingdom) 1996; 4: 6-11.
[32] Guenet JM. Macromolecular Symposia 1997; 114: 97-108.
[33] Boyer RF, Baer E, Hiltner A. Macromolecules 1985; 18: 427-34.
[34] Pines E, Prins W. Macromolecules 1973; 6: 888.
[35] Feke GT, Prins W. Macromolecules 1974; 7: 527-30.
[36] Pritchard JG. Poly(vinyl alcohol) Basic properties and uses London: Gordon and Breach, Science Publishers Ltd., 1970.
[37] Yao L, Haas TW, Guiseppi-Elie A, Bowlin GL, Simpson DG, Wnek GE. Chemistry of Materials 2003; 15: 1860-1864.
[38] Koski A, Yim K, Shivkumar S. Materials Letters 2004; 58: 493-497.
[39] Zeng J, Hou H, Wendorff JH, Greiner A. Polymer Preprints (American Chemical Society, Division of Polymer Chemistry) 2003; 44: 174-175.
[40] Based on published data, the entanglement molecular weight of PVA is assumed to 3750 gm/mol.
[41] Aharoni SM. Macromolecules 1983; 16: 1722-8.
[42] Aharoni SM. Macromolecules 1986; 19: 426-34.
[43] Wool RP. Macromolecules 1993; 26: 1564-1569.
[44] Komatsu M, Inoue T, Miyasaka K. Journal of Polymer Science, Part B: Polymer Physics 1986; 24: 303-11.
[45] For details of the experimental setup, the reader is referred to previous publications from our group (e.g. references 4, 22 or 37 in this paper). Poly(vinyl alcohol oxide) (PVA) (catalog # 36314-6; Mw = 85-146k), For the electrospinning experiment, PVA solutions (6, 8 and 10 wt% in deionized water was prepared by heating the solution to 95C. In a typical experiment, a solution of polymer was drawn into a 5 ml syringe with a blunt needle at the end. The syringe with the needle was attached to the syringe pump (kdScientific, New Hope, PA). A high voltage supply (CZE 1000R) obtained from Spellman, NY was employed to obtain a field by connecting it to the blunt needle. The voltage was fixed at 25 kV and the source to target distance was kept at 20 cm for the PVA/water solutions. The flow rate was fixed at 4 ml/hr. In order to obtain fibers for visualization by optical microscopy, the fibers were collected on glass slides covering a grounded metal target rotating at approximately 750-1000 rpm. Optical micrographs were obtained using an Olympus optical microscope (Olympus BE201).
[46] Sato T, Okaya T. Polymer Journal (Tokyo, Japan) 1992; 24: 849-56.
[47] Lee KH, Kim HY, La YM, Lee DR, Sung NH. Journal of Polymer Science, Part B: Polymer Physics 2002; 40: 2259-2268.
[48] Gupta P, Wilkes GL. Polymer 2003; 44: 6353-6359.
[49] Doty P, Wagner H, Singer S. Journal of Physical and Colloid Chemistry 1947; 51: 32-57.

[50] Abied H, Brulet A, Guenet JM. Colloid and Polymer Science 1990; 268: 403-13.
[51] There is some discrepancy in the published data for the entanglement molecular weight of PVC. The two most commonly reported values are 3125 gm/mol [41,42] and 5500 gm/mol [43]. For our calculations, we have employed the mean i.e. 4310 gm/mol.
[52] Poly(vinyl chloride) (PVC) (Mw = 233k, catalog # 346764; Mw=106k, catalog # 346756) and solvents such as tetrahydrofuran, morpholine and dioxane were all obtained from Aldrich. The higher Mw PVC (Geon 407; Mw unknown) was donated by PolyOne. For the electrospinning experiment, PVC/THF, PVC/morpholine and PVC/dioxane solutions of different concentrations as described in the text were also prepared by heating the solutions to 70°C. A voltage was adjusted to 15 kV and the tip to target distance of 20 m was employed. The flow rate was fixed at 4 ml/hr. In order to obtain fibers for visualization by optical microscopy, the fibers were collected on glass slides covering a grounded metal target rotating at approximately 750-1000 rpm. Optical micrographs were obtained using an Olympus optical microscope (Olympus BE201).
[53] Keller A. Faraday Discussions 1995: 1-49.
[54] Soenen H, Berghmans H. Journal of Polymer Science, Part B: Polymer Physics 1996; 34: 241-7.
[55] Hong PD, Huang HT. European Polymer Journal 1999; 35: 2155-2164.
[56] Hong PD, Chou CM, He CH. Polymer 2001; 42: 6105-6112.

Table 1. Compilation of PVA electrospinning results and entanglement number

Reference	M_w x 10^3 (gm/mol)	degree of hydrolysis (%)	concentration (wt%)	morphology	$(n_e)_{soln}$ [§]
Koski et al.	9-10	98-99	25	f + b	0.55
	9-10	98-99	35	f	0.8
	13-23	98	21	f + b	0.82
	13-23	98	25	f	1
	13-23	98	27	f	1.1
	13-23	98	31	f	1.3
	31-50	98-99	25	f	2.2
	50-85	97	9	f	1.3
	50-85	97	11	f	1.6
	50-85	97	13	f	1.9
	50-85	97	17	f	2.5
	124-186	>99	6	f + b	1.95
Yao et al.	115	>99	10	f *	2.4
Zeng et al.	100	98	6	f + b	1.2
	100	98	8	f + b	1.7
	125	98	6	f + b	1.6
	125	98	8	f	2.1
	195	98	6	f	2.4
	195	98	8	f	3.3
This work	115	>99	6	f + b	1.4
	115	>99	8	f + b	1.9
	115	>99	10	f	2.4

[§] The mean M_w is used whenever molecular weight range is given

* Only upon addition of surfactant

Table 2. PVC electrospinning results

System	M_w (true) x 10^3(gm/mol)	Observed concentration (wt%)	Predicted concentration (wt%)	Morphology	$(n_e)_{soln}$*
PVC/THF	249	6	5.5[a]	f + b	2
	249	9	9.5[b]	f	3.2
	210	7	6.4[a]	f + b	2
	210	11	10.8[b]	f	3.2
	91	10	14.2[a]	f	1.3
	91	16	23.7[b]	f	2.1
PVC/Morpholine	249	3.5	8[b]	f	1.3
	249	4.5	8[b]	f	1.7
	210	5	9.4[b]	f	1.7
	91	7	21[b]	f	1.04
PVC/Dioxane	210	1	5.8[a]	b	0.3
	210	3	5.8[a]	b	0.9

[a] refers to predicted concentration where fiber formation should be first observed
[b] corresponds to predicted concentration where only fibers are expected
* calculated using the experimental values i.e. column 3

Table 3. Heating effects on PVC molecular weight

M_w x 10^3 gm/mol*	GPC data obtained in our laboratory		
	before heating	after heating	96 hrs after heat treatment
106	108	91	91
233	251	210	208
na[§]	343	249	260

* Values reported by supplier (Aldrich Chemicals)
§ No value was available from supplier (PolyOne Chemicals)

Figure Legends

Figure 1. Optical micrographs of structure obtained by electrospinning PVA/deionized water solutions heated to 95°C and cooled to room temperature (a) 6 wt% (b) 8 wt% and (c) 10 wt%. The corresponding morphologies 45 minutes after cooling to room temperature are shown in (d) 6 wt% (e) 8 wt% and (f) 10wt%.

Figure 2. Effect of heat treatment (70°C) on the morphology of electrospun fibers from a 9 wt% PVC/THF solution (Mw = 249k) (a) before heating and (b) after heat treatment for 10 minutes.

Figure 3. Electrospinning of PVC (M_w = 191k)/THF solutions: (a) 6.3 wt% and (b) 11 wt%.

Figure 4. Electrospinning of PVC (M_w = 85k)/THF solutions: (a) 10 wt% and (b) 16 wt%.

Figure 5. Determination of the critical Mw for PVC/THF solutions where fiber formation mechanism changes from simply physical entanglements to a combination of entanglements and thermoreversible gelation of takes place. The dashed line is corresponds to $(\phi_g)_{threshold}$ calculated using equation 4 while the bold line is $(\phi_{el})_{fiber}$ calculated using equation 5.The experimental values of $(\phi_g)_{threshold}$ (▲) and $(\phi_{el})_{fiber}$ (□) have been plotted for comparison.

Figure 6. Effect of time on electrospinning 4 wt% PVC (M_w = 191k)/Morpholine solutions: (a) immediately on cooling and (b) 48 hours after cooling to room temperature.

Figure 7. Electrospinning 5 (a, c) and 6 (b, d) wt% PVC (M_w = 191k)/Morpholine solutions as a function of time: (a) 5 wt% immediately on cooling, (b) 6 wt% immediately on cooling (c) 5 wt% solution 24 hours after cooling to room temperature (d) physical gelation of 6 wt% solution.

Figure 8. Electrospinning of PVC/dioxane (M_w = 191k) solutions (a) 1 wt% and (b) 3 wt% immediately upon cooling.

Figure 1. Optical micrographs of structure obtained by electrospinning PVA/deionized water solutions heated to 95°C and cooled to room temperature (a) 6 wt% (b) 8 wt% and (c) 10 wt%. The corresponding morphologies 45 minutes after cooling to room temperature are shown in (d) 6 wt% (e) 8 wt% and (f) 10wt%.

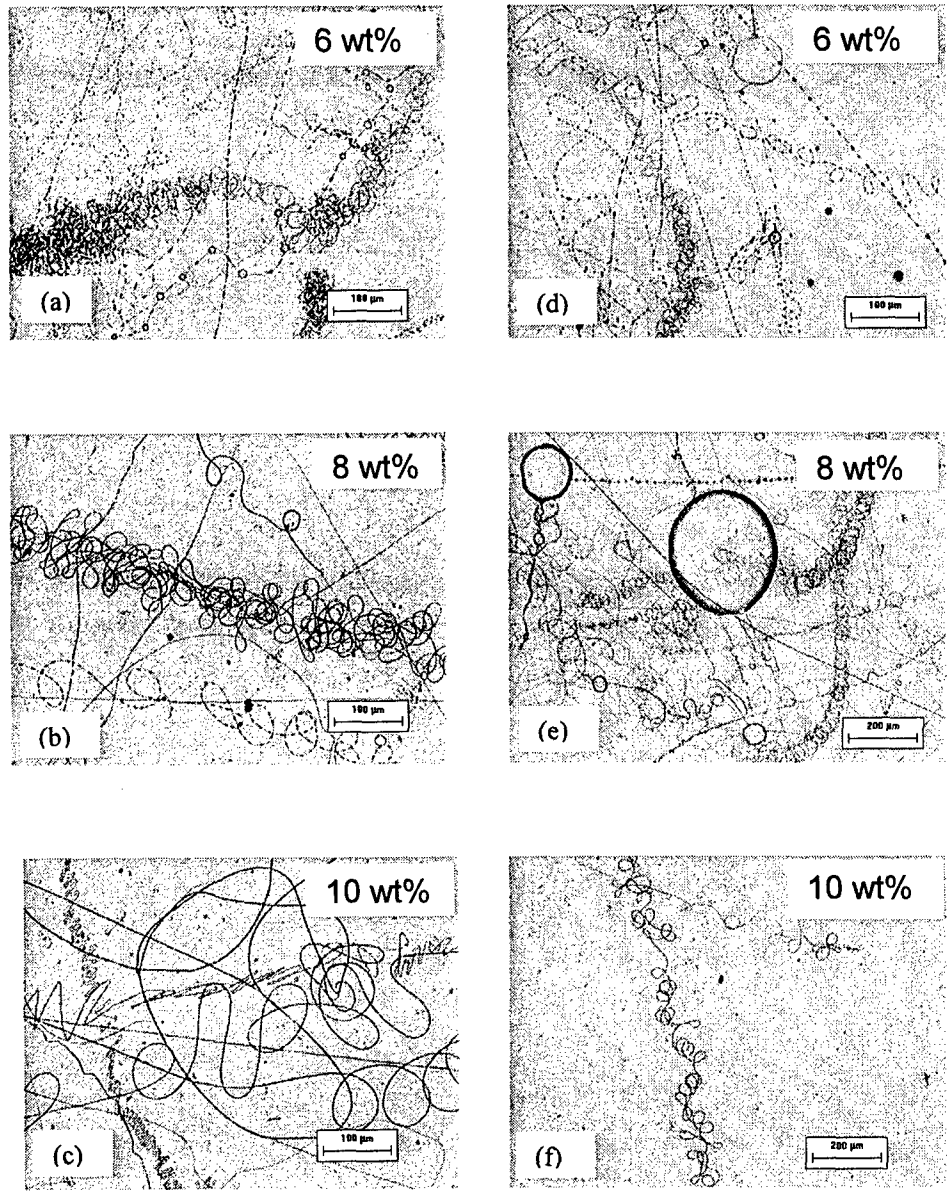

Figure 2. Effect of heat treatment (70°C) on the morphology of electrospun fibers from a 9 wt% PVC/THF solution (Mw = 249k) (a) before heating and (b) after heat treatment for 10 minutes.

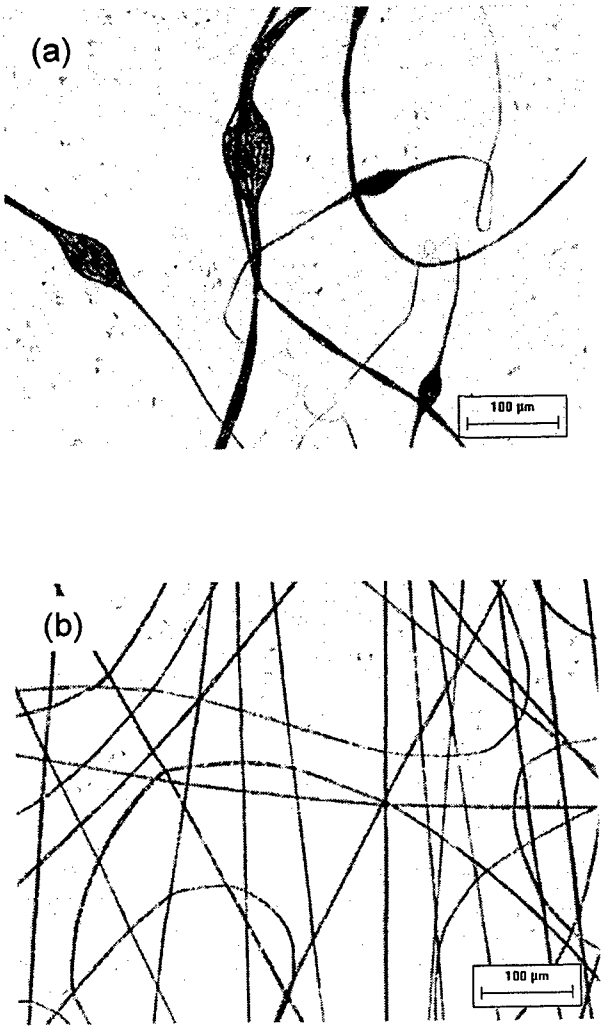

Figure 3. Electrospinning of PVC (M_w = 191k)/THF solutions: (a) 6.3 wt% and (b) 11 wt%.

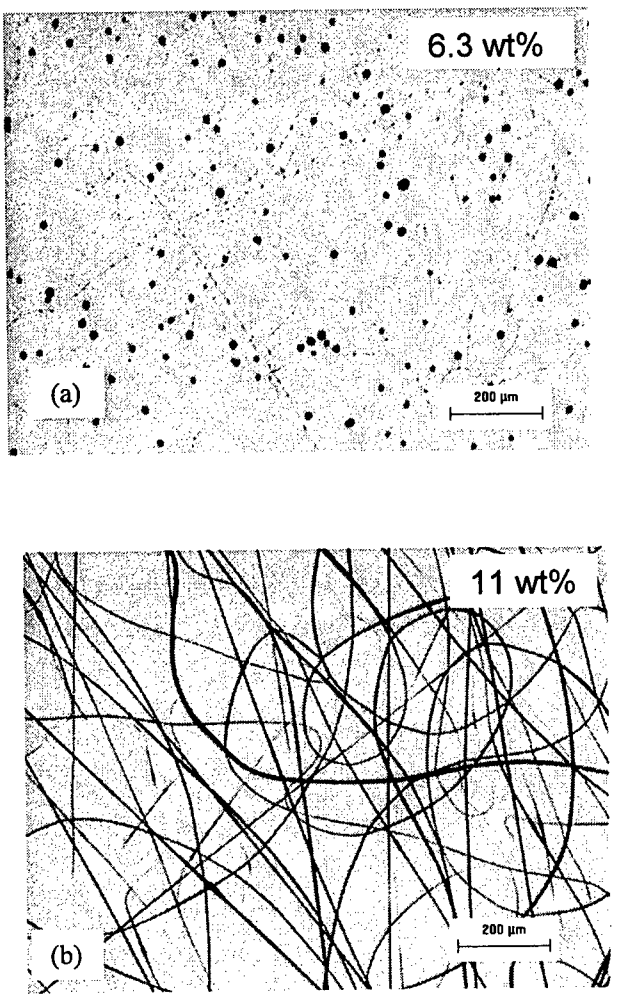

Figure 4. Electrospinning of PVC (M_w = 85k)/THF solutions: (a) 10 wt% and (b) 16 wt%.

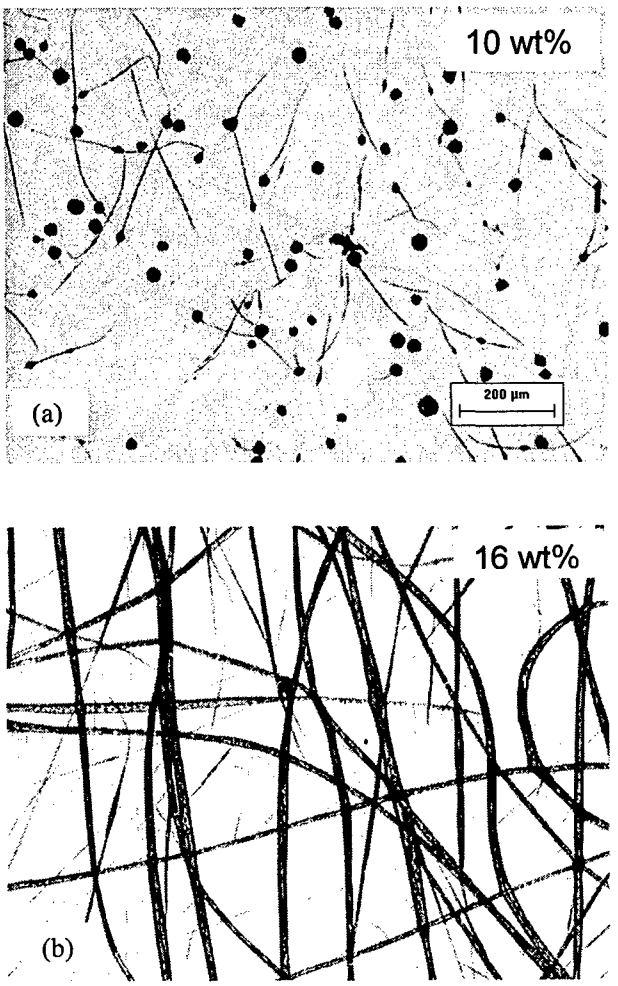

Figure 8. Determination of the critical M_w for PVC/THF solutions where fiber formation mechanism changes from simply physical entanglements to a combination of entanglements and thermoreversible gelation of takes place. The dashed line is corresponds to $(\phi_g)_{threshold}$ calculated using equation 4 while the bold line is $(\phi_{el})_{fiber}$ calculated using equation 5.The experimental values of $(\phi_g)_{threshold}$ (▲) and $(\phi_{el})_{fiber}$ (□) have been plotted for comparison. The critical M_w for mechanism crossover is approximately 155k. Above this M_w, fiber formation mechanism in PVC/THF is primarily due to physical entanglements.

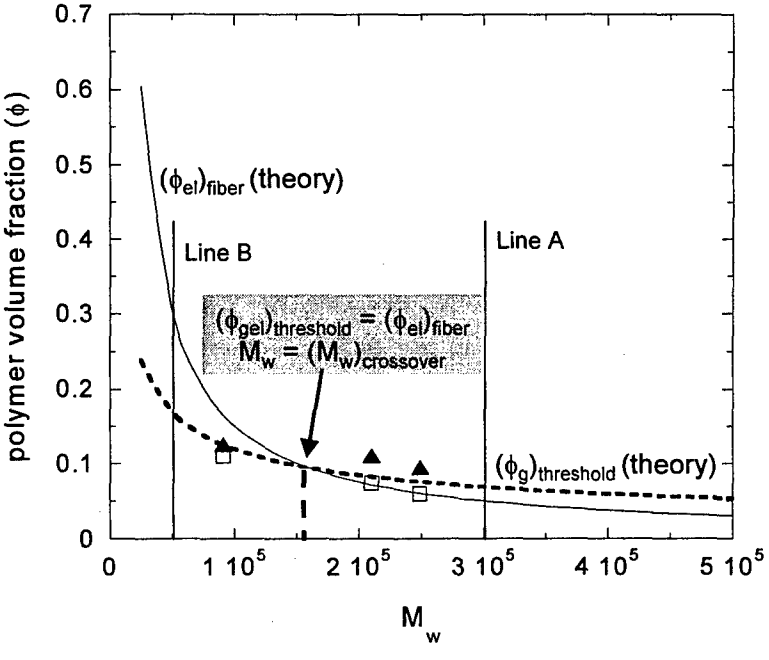

Figure 6. Effect of time on electrospinning 4 wt% PVC (M_w = 191k)/Morpholine solutions: (a) immediately on cooling and (b) 48 hours after cooling to room temperature.

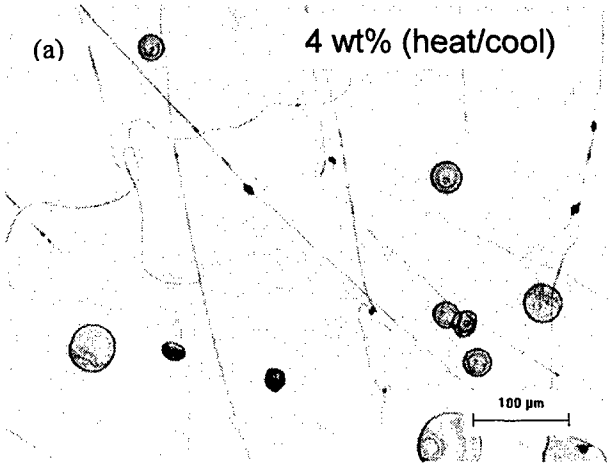

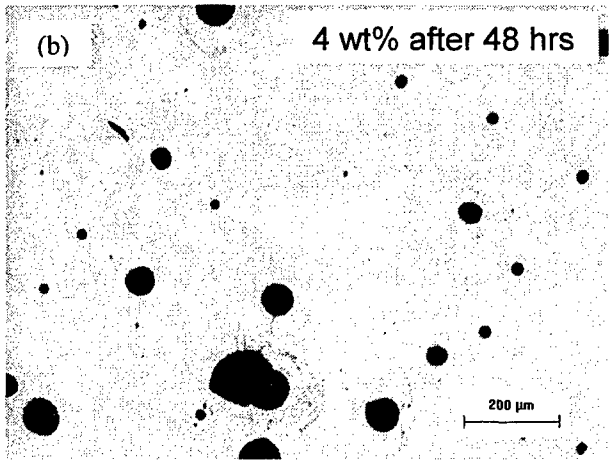

Figure 7. Electrospinning 5 (a, c) and 6 (b, d) wt% PVC (M_w = 191k)/Morpholine solutions as a function of time: (a) 5 wt% immediately on cooling, (b) 6 wt% immediately on cooling (c) 5 wt% solution 24 hours after cooling to room temperature (d) physical gelation of 6 wt% solution.

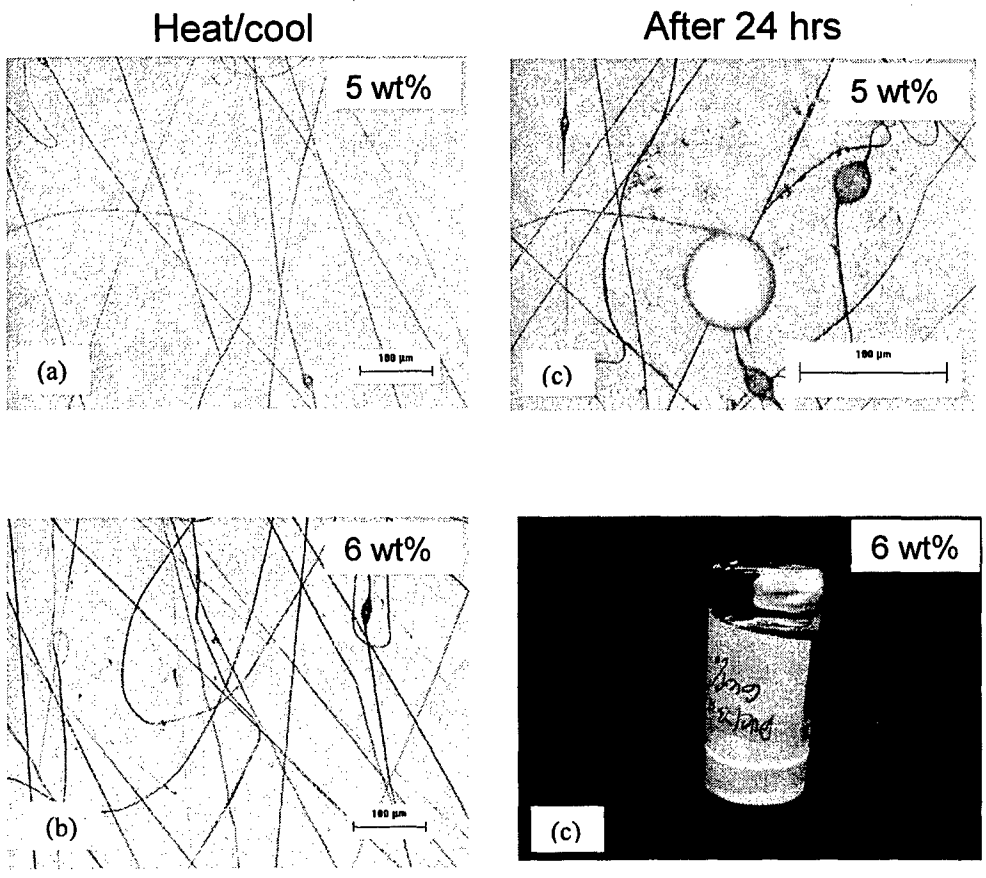

Figure 8. Electrospinning of PVC in dioxane (a) 1 wt% and (b) 3 wt% immediately upon cooling.

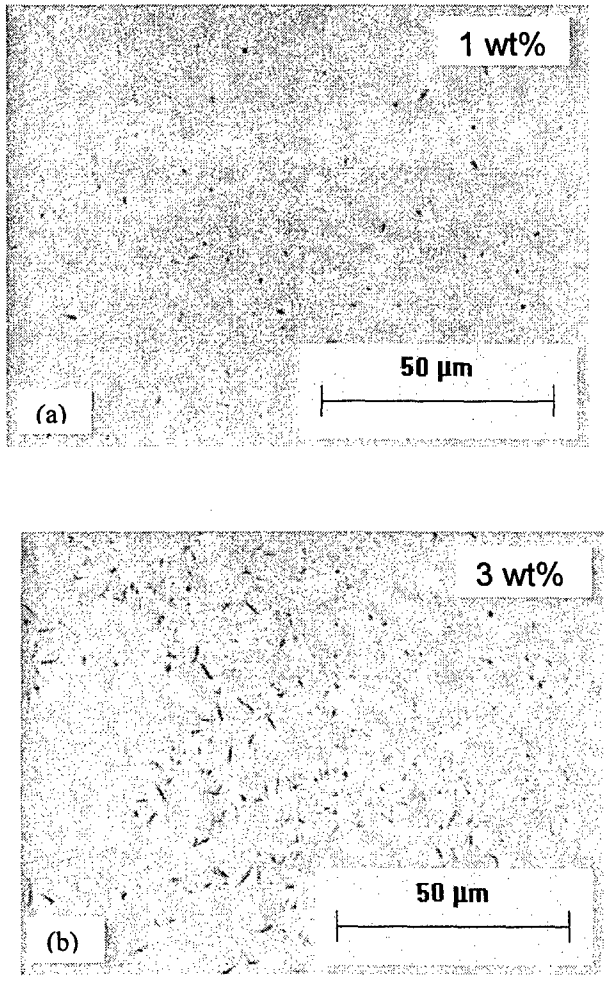

Fabrication of Aligned Electrospun Mats by Suppression of Bending Instability

Suresh L. Shenoy,[a]* W. Douglas Bates[a] and Gary E. Wnek[b]*

Contribution from:

[a] Chemical and Life Sciences Engineering
Virginia Commonwealth University
Richmond, VA 23284-3028

[b] Currently at:
Department of Chemical Engineering
Case Western Reserve University
Cleveland, OH 44106-7217

* Corresponding author: Suresh Shenoy: sshenoy@vcu.edu

Abstract

Fabricating aligned electrospun fibers is a topic of interest, especially in biomedical, electrical and optical applications. In this work, we present a method for obtaining aligned fibers. The technique consists of counter-balancing the electrical forces (which are necessary to overcome solution surface tension and subsequent jet ejection) with viscoelastic forces. Excessive coulombic forces frequently enhance jet bending instabilities that yield non-woven fibrous mats; however, by compensating for the electrical forces with sufficient viscoelastic forces, a stable, linear jet is produced. This can be achieved by lowering the applied voltage to reduce surface charges on ejected jet fibers in combination with judicious choice of polymer concentration and/or molecular weight. We have applied this technique to numerous polymer/solvent systems and have obtained aligned electrospun mats. In general, we electrospun polymers that are glassy or semi-crystalline at room temperature, which rapidly lose solvent and are collected 'dry', and have fiber diameters > 1 μm.

Keywords: electrospinning; fiber alignment, viscoelasticity

1. Introduction

Electrospinning is a convenient way to obtain non-woven mats consisting of ultrafine fibers [1-3]. In recent years, electrospun mats of a variety of synthetic and biological polymers with fiber diameters ranging from tens of microns to tens of nanometers have been employed for applications ranging from filtration to tissue engineering and wound dressing [1,4-9]. Typically, in electrospinning, under the influence of an applied voltage, the ejected liquid jet follows a chaotic motion as it travels towards the target due to repulsive forces between the similarly charged elements on the fiber [10-12]. Consequently non-woven mats without any preferential fiber alignment are obtained.

For some potential applications, such as tissue engineering, certain optical and electronic applications, fiber alignment may be desirable [13-16]. As a result, a number of groups have been investigating mechanisms to obtain aligned polymer fibers by electrospinning [17-28]. One method employed by many laboratories including our own is the use of a rotating drum as the target [8,24,27-29]. It has been suggested that the degree of fiber alignment is a function of the drum speed, and at higher rotation rates, highly aligned fibers will be achieved [8,25]. However, often we have observed that after a uniform layer of aligned fibers is formed on the drum surface, the residual charge on the deposited fibers inhibit fiber alignment for the subsequent layers.

Alternative techniques have been employed including an electrostatic 'focusing' lens. Specifically, concentric rings are used to dampen the bending instability and inhibit the chaotic motion of the ejected jet [28]. An additional method involves rotating disk collectors with sharp edges, which are used to obtain both preferential alignment and formation of nanofiber crossbars [18,20,21]. The sharp edges of the rotating disk serves to focus the electric field lines thereby allowing fiber alignment. Recently, Sundaray, *et al.* [21] combined two techniques (rotating drum + sharp counter electrode on the drum) to obtain aligned polystyrene (PS) and poly(methyl methacrylate) (PMMA) fibers on a flexible plastic substrate. The authors speculated that alignment was primarily due to reduced syringe/target distance, high polymer concentration and use of sharp pin as the counter electrode, which helps to focus the electric field configuration. Finally, Li, *et al.* [22,23] fabricated uniaxially aligned arrays of polymeric and ceramic fibers using two pieces of conductive silicon strips separated by a void gap. The advantage of this setup

is the ability to transfer aligned fibers from one surface to another. In this communication, we report that fabricating electrospun mats with good fiber alignment can be obtained by employing lower applied voltages in combination with judicious choice of polymer/solvent systems, and to a smaller degree, reducing the polymer solution flow-rate at the source.

2. Experimental

The polymer/solvent systems are carefully chosen to illustrate the general applicability of this technique [30]. A typical electrospinning experiment is shown in Figure 1 [31]. A disposable polypropylene (PP) syringe with a blunted stainless-steel needle tip was charged with ~5-10 mL of polymer solution and placed in a syringe pump (kdScientific, New Hope, PA). Specifically, the polymer concentration was chosen to enable fiber formation [32]. Application of an appropriate voltage using a high voltage power supply (CZE 1000R, Spellman, NY) to the syringe needle, resulted in a stable jet, which was ejected and collected on a home-built oscillating/rotating stainless-steel mandrel (10 cm diameter, 100-200 rpm) located 25 cm from the syringe tip (except for PEO, where this distance was adjusted to 15 cm). Table 1 summarizes the polymer/solvent systems, polymer molecular weights, polymer concentrations, and applied voltages used in this work, in addition to the observation of fiber alignment.

3. Results

Differences in fiber alignment are clearly illustrated in Figure 2 for electrospun mats of 32 wt% polystyrene (PS)/tetrahydrofuran (THF) solutions in the absence (Figure 2A) and presence of salt (0.2 wt% lithium bromide (LiBr); Figure 2B). The applied voltages are the same for both samples (10 kV over a 25 cm source-to-target distance). Based upon an average PS fiber diameter of ~10 μm, the electrospun mats are estimated to consist of ~8 (non-woven, in presence of LiBr) and ~13 (aligned, no LiBr present) layers of fibers. The observation of 13 layers of aligned fibers is significant. As mentioned earlier, typically, fiber alignment becomes less uniform as layers build-up on the mandrel due to charge repulsion between fibers. In addition, the observed electrospinning jet in the absence of salt is a single steady jet without the commonly observed bending instabilities (bending instability and steady jets are illustrated in Figures 1A and 1B, respectively). In fact, increasing the applied voltage (by as much as 10 kV) did not disrupt the jet or initiate bending instability. Moreover, electrospinning from dichloromethane

(DCM, 27 wt% PS) resulted in aligned fibers, as did electrospinning higher molecular weight PS (280k) from THF at lower concentrations (22 wt%). In both instances, aligned fibers (8-10 μm diameter) were obtained. It should be noted that other systems have been observed to behave in a similar manner. For instance, Theron, *et al.* [33] has reported that for polyethylene oxide (PEO)/water and PEO/water/ethanol solutions, uniform stable (straight) jets are observed.

In contrast, adding a small amount of LiBr results in bending instabilities even at minimal applied voltages (Figure 2B). Note that it is accepted that addition of a salt can aid the formation of an 'electrospinnable' polymer solution at considerably lower polymer concentrations [34]. In the present case, even under conditions (e.g. applied voltage, high polymer concentration) that are identical to those employed for no salt, chaotic whipping behavior is observed and non-woven mats are obtained. Interestingly, addition of 8 μm copper flakes to PS/THF solutions does not result in jet instability contrary to the results obtained for PS/LiBr/THF, and consequently, aligned copper/PS composite fibers are obtained. The PS encapsulates the copper flake, and the resulting non-conductive fibers exhibit beaded fiber morphology (not shown).

Although not shown, 14 wt% polymethylmethacrylate (PMMA)/THF solutions produce aligned electrospun fibers over a range of applied voltages (Table 1). The fiber diameters are similar to those obtained for PS/THF aligned systems (~8-10 μm), and calculations indicate that ~6 layers are aligned. In PS and PMMA aligned mats, the high degree of fiber alignment produces an interesting transparency effect (Figures 2C and 2D). In this case (Figure 2C), transparency or the ability to see the images depends on the amount of transmitted light from the object (images) to the eye and is a function of fiber alignment in the electrospun mat. As shown in Figure 2C, the aligned PS fiber mat (130 μm thick) allows light transmission when placed up to ¼" of the object (image). At distances > ½" the aligned mat acts as a filter and does not permit light transmission (not shown) due to light scattering. In contrast to Figure 2C, an opaque non-woven PS mat electrospun from PS/THF solution that contained 0.2 wt% LiBr is displayed in Figure 2D. Despite the lower thickness of the nonaligned mat (85 μm vs. 130 μm for aligned) none of the images are visible due to light scattering in non-woven mats (i.e. no transmission).

In a similar study, a series of polymers that are structurally similar to PS, but with polar aromatic structures (poly(2vinyl pyridine)(P2VP), poly(4vinylpyridine) (P4VP) and poly(vinylpyrrolidone) (PVP) were chosen to determine the generality of electrospinning aligned fibers for 'glassy' polymers. Unlike PS and PMMA, these polymers exhibited different mat

morphologies based upon the applied voltages (Table 1). At voltages just above the critical point (in this instance, 5 kV is sufficient to overcome surface tension), aligned fibers were observed; however, at higher voltages, bending instability behavior is observed resulting in non-woven mats. Additionally, the aligned fibers appear to retain significant amounts of residual charge even at low applied voltages. Attempts to prepare samples for SEM results in the topmost layers of fibers becoming disordered apparently by columbic attractions to the SEM sample holder or tweezers. Similar strong electrostatic attractions are not observed for PS or PMMA.

Following these initial studies, and given our interest in biocompatible/biodegradable tissue scaffolds [4,35-38], attempts were made to align semi-crystalline poly(l-lactic acid) (PLLA) and amorphous poly(lactic acid-co-glycolic acid) (PLGA; 75:25 lactic:glycolic acid). Shown in Figure 3 are representative SEM images for 20 wt% PLGA fibers electrospun from DCM at low applied voltages (Figure 3A, 7 kV, aligned) and high applied voltages (Figure 3B, 20 kV, randomized). Similar results were obtained for PLLA fibers (Table 1). Interestingly, for PLGA, at low magnification (100 μm) for an applied voltage of 20kV, we observe regions where some degree of fiber alignment maybe present (Figure 3C). However at higher magnifications (10 μm), the random nature of the electrospun fiber mats (Figure 3B) becomes clear. At a still higher voltage (28 kV, not shown), a completely non-woven mat was obtained. The transparent aligned mat obtained from PLGA (7 kV) is shown in Figure 3D and displays a remarkable clarity (even more so than the transparent PS mat shown in Figure 2C). Note that light transmission in composites having dispersed particles or unidirectional fibers (aligned, obtained by conventional spinning techniques) has been previously investigated [39-42] and has been observed to be a function of fiber diameter (or particle size) and mat thickness.

Using the composites analogy, whether the increased clarity in PLGA mats is a result of the slightly thinner fibers (5 μm) and/or a significantly thinner mat (30 μm) with much fewer fiber layers (~ 6) is currently being investigated. For PLLA mats, transparency of the electrospun mats is quite poor despite fiber alignment. Thus transparency is restricted to amorphous polymers such as PS, PMMA or PLGA. On the other hand, aligned mats of PLLA or PEO do not exhibit this behavior due to light scattering by microcrystallites.

Lastly, we have repeated the results of Theron, *et al.* [33] by electrospinning PEO from H_2O (Table 1). In this instance, we shortened the source-to-target distance to 15 cm because at 25 cm the fibers had a tendency to stray from the rotating target. The PEO mats align at lower

applied voltages; however, generating thick mats of aligned fibers is difficult due to the tendency of PEO fibers to retain some water (at the smaller source-to-target distance) and fuse, thereby forming films instead of electrospun mats.

4. Discussion

In electrospinning, for a constant source to target distance, the applied voltage affects the entire spinning process from jet initiation to jet instability. For jet initiation, the charge repulsion on the drop (Taylor cone) surface overcomes the surface tension. In the later stages, as the liquid jet accelerates towards the target under the influence of the electric field, charge repulsion between various elements of the jet can result in bending instability [10,11]. Thus the ejected liquid jet undergoes a chaotic motion as it accelerates towards the target (see Figure 1A). The surface charge density and the jet radius (away from the nozzle) may be critical parameters, which determines the commencement of bending instability. It appears from our own experiments that viscoelasticity of the polymer solution has a stabilizing effect which is in agreement with the operating diagrams suggested by Hohman et al. [43,44] (see Figure 15 and 16 in reference 44).

For PS and PMMA, we observed a steady jet (see Figure 1B), which resulted in significant fiber alignment in the electrospun mats. Increasing the applied voltage by 8-10 kV did not affect the steady jet by initiating bending instabilities, probably due to lower surface charge density. On the other hand, for P2VP and PVP solutions, the jet exhibits whipping or bending instability at higher voltages (14kV), we believe due to a higher charge density. Consequently electrospun mats exhibit no anisotropy (alignment). Interestingly note that except for the presence of the N atom in the aromatic ring (which makes it more polar), the repeat unit of P2VP and P4VP are quite similar to PS. When the applied voltage is decreased to 6kV, we were able to maintain a steady jet (Figure 1B) and correspondingly obtain aligned mats. The appearance of the steady jet for P2VP and P4VP at lower voltages is probably due to the reduction in repulsion between fiber elements, which is a result of lower surface charges. Remarkably, it is possible to observe the change from a steady straight jet regime to a whipping/bending chaotic jet for P2VP and P4VP solutions as the applied voltage is increased from 6 kV to 9 kV.

The above hypothesis also appears to explain the lack of fiber alignment in the electrospun mats for PS with a small amount of LiBr. Addition of LiBr increases fluid

conductivity (ionic) and hence surface charge density. This results in increased repulsion and domination of the chaotic whipping motion and hence formation of a non-woven mat. This validates the arguments put forth by Hohman et al. [43,44] in the form of theoretical operating diagrams (see Figures 15 and 17in reference 44). Briefly, operating diagrams (predictions) for PEO/water/KBr show that the region of bending instability increases significantly while that of steady jet decreases as solution conductivity (or surface charge density) is increased. From an experimental perspective, the behavior of PLLA and PLGA solutions further corroborates this hypothesis. At lower voltages, and hence lower surface charge density, perfectly aligned fiber mats are obtained. Increasing the surface charge by applying a higher voltage disrupts the steady jet by introducing bending instability and therefore fiber alignment. Note that in contrast to P2VP and P4VP, for PLLA and PLGA the chaotic jet formed at the higher voltage (e.g. 20 kV for PLGA) is interspersed with the presence of a straight jet. This results in regions where some fiber alignment is present (observed for $\geq$ 100 μm) but not on a local scale (~10 μm). At still higher voltages (28 kV), the liquid jet ejected from the Taylor cone follows a predominantly chaotic motion resulting in a non-woven mat. For PEO solutions, analogous to PS and PMMA, the steady jet regime in PEO solutions appears to hold, even at extremely high voltages. Thus the ability of the polymer to hold surface charge is a key factor in obtaining a steady straight jet. Our experiments suggest that obtaining a straight jet for polar polymers (P2VP, P4VP, PVP) is a more difficult task in contrast to nonpolar polymers such as PS.

Besides the polymer repeat unit, solvent will also play an important role in the ability to maintain a steady straight jet. Preliminary experiments appear to back this hypothesis. Figure 4 shows the SEM of PS mats electrospun from THF (Figure 4A same as Figure 2A) and dimethylformamide (DMF). Specifically PS was chosen so that only solvent polarity affects ejected jet charge density. Note that the dielectric constant of DMF is considerably higher than THF (~ 38.25 vs. 7.52) [45]. Clearly Figure 4 shows that solvent dielectric constant has a significant effect on fiber alignment. Thus surface charge effects are substantial in DMF thus producing chaotic jet motion and consequently a non-woven mat (Figure 4B). Another possible reason could be differences in solvent volatility ($T_{BP,DMF}$ = 153°C; $T_{BP,THF}$ = 65°C). However in preliminary experiments, we were able to obtain aligned mats (not shown) from cyclohexanone (dielectric constant = 16.1, T_{BP} = 155°C [45]). Thus fiber alignment (or lack of) in THF and DMF appear to be a result of the differences in the dielectric constant. In summary, we believe

that both polymer and solvent polarity (dielectric constant) affect the ability to obtain a steady jet. Thus at higher voltages non-woven mats are obtained when either the polymer (e.g. P2VP/DCM) or solvent polarity/dielectric strength (e.g. PS/DMF) exceeds a threshold value. We are currently in the process of determining this threshold value and the relationship between polymer/solvent dielectric constant, applied voltage and fiber alignment. Besides the polymer/solvent polarity, some other parameters that can affect fabrication of aligned electrospun mats are discussed below.

Preliminary results suggest that the effect of solvent volatility and flow rate on fiber alignment is not significant. Though not reported here due to space constraints, we have also obtained aligned electrospun mats of PS and P2VP from DCM. Here a few observations on volatility and flow rate are given. For volatile solvents such as DCM (T_{BP} = 40°C [45]), low flow rates can cause tip blockage as the solvent evaporates rapidly. If the flow rate is high, there appears to be significant wastage of polymer solution by dripping. In theory, this can be avoided by increasing the applied voltage. However, the increased voltage would result in bending instability. We also noticed that at high flow rate and applied voltage, multiple jets are ejected from the cone; one from the tip and others from the side of the Taylor cone. This can dramatically decrease fiber alignment due to increased possibility of repulsive forces acting on the fibers. Thus the flow rate and applied voltage have to be optimized to ensure formation of a stable Taylor cone and ejection of a single jet from the cone.

In order to ascertain the role of molecular weight on fiber alignment in electrospun mats, we employed a higher molecular PS (280k versus 190k) using THF as the solvent. Note that for higher M_w, polymer concentration needed for fiber formation is lower (24 wt% versus 30 wt%). No notable differences were observed between the fiber alignments for the two M_w's. On the other at lower concentration (22 wt%), where a small amount of beaded fibers were obtained, jet was stable only for short periods of time before it would develop bending instabilities. In principle lowering the applied voltage could help dampen or reduce the bending instability. However in this case, inability of the jet to reach the target at lower voltages is a problem. In summary based on the preliminary observations on PS, PMMA, P2VP, P4VP, PLLA, PLGA and PEO systems it appears that obtaining a steady jet is a balance between the viscoelastic forces and the repulsive columbic forces. Thus for a given polymer concentration, higher molecular

weight resulting in increased viscoelastic stresses could stabilize the single jet for PEO jets. Alternatively for a given M_w, higher concentrations could accomplish the same end result.

Finally we discuss the effect of the rotational speed of the drum [27,29] and fiber collection efficiency. Below a critical drum speed obtaining aligned fibers is almost impossible. Our observations indicate that as the drum speed is decreased below a critical value, maintaining a steady jet is impossible. We believe this a result of the repulsion from the already deposited fibers. For PS and PMMA, we observed that when the drum is stationary, in the initial stages prior to any significant fiber deposition, we were able to obtain a steady single jet. As fiber deposition on the stationary drum proceeded, maintaining this steady jet became difficult. After a certain critical amount of fibers were deposited, a single jet could no longer be obtained.

In conclusion, we have been able to obtain aligned electrospun mats of a number of polymers by optimizing the applied voltage, concentration/molecular weight to reduce surface charge density and increase the stabilizing viscoelastic forces. However a significant drawback of this technique is that the resulting fiber diameters are ≥ 1 μm. The reason for these diameters is the high polymer concentrations/M_w needed to provide the stabilizing viscoelastic forces to overcome the charge repulsion. We are currently in the process of investigating the effect of polymer/solvent polarity on fiber alignment and use this knowledge to apply the technique described here to obtain aligned nanofiber electrospun mats.

Acknowledgements. The authors would like to thank DARPA (Bio-Optic Synthetic Systems Program) and the NASA Office of Space Sciences for generous support.

References and Notes

[1] Huang ZM, Zhang YZ, Kotaki M, Ramakrishna S. Composites Science and Technology 2003; 63: 2223-2253.

[2] Frenot A, Chronakis IS. Current Opinion in Colloid & Interface Science 2003; 8: 64-75.

[3] Doshi J, Reneker DH. Journal of Electrostatics 1995; 35: 151-160.

[4] Boland ED, Matthews JA, Pawlowski KJ, Simpson DG, Wnek GE, Bowlin GL. Frontiers in Bioscience 2004; 9: 1422-1432.

[5] Boland ED, Wnek GE, Simpson DG, Pawlowski KJ, Bowlin GL. Journal of Macromolecular Science-Pure and Applied Chemistry 2001; 38: 1231-1243.

[6] Kim SH, Nam YS, Lee TS, Park WH. Polymer Journal 2003; 35: 185-190.

[7] Layman JM, Kenawy ER, Watkins JR, Carr ME, Bowlin GL, Wnek G. 226th ACS National Meeting 2003: U436-U436.

[8] Matthews JA, Wnek GE, Simpson DG, Bowlin GL. Biomacromolecules 2002; 3: 232-238.

[9] Wnek GE, Carr ME, Simpson DG, Bowlin GL. Nano Letters 2003; 3: 213-216.

[10] Yarin AL, Koombhongse S, Reneker DH. Journal of Applied Physics 2001; 89: 3018-3026.

[11] Shin YM, Hohman MM, Brenner MP, Rutledge GC. Polymer 2001; 42: 9955-9967.

[12] Reneker DH, Yarin AL, Fong H, Koombhongse S. Journal of Applied Physics 2000; 87: 4531-4547.

[13] Yang F, Murugan R, Wang S, Ramakrishna S. Biomaterials 2005; 26: 2603-2610.

[14] Lee CH, Shin HJ, Cho IH, Kang Y-M, Kim IA, Park K-D, Shin J-W. Biomaterials 2004; 26: 1261-1270.

[15] Eastin J, Vu D, Larsen G. Abstracts of Papers, 229th ACS National Meeting, San Diego, CA, United States, March 13-17, 2005 2005: BIOT-362.

[16] Li D, Xia Y. Advanced Materials (Weinheim, Germany) 2004; 16: 1151-1170.

[17] Katta P, Alessandro M, Ramsier RD, Chase GG. Nano Letters 2004; 4: 2215-2218.

[18] Zussman E, Theron A, Yarin AL. Applied Physics Letters 2003; 82: 973-975.

[19] Xu CY, Inai R, Kotaki M, Ramakrishna S. Biomaterials 2003; 25: 877-886.

[20] Theron A, Zussman E, Yarin AL. Nanotechnology 2001; 12: 384-390.

[21] Sundaray B, Subramanian V, Natarajan TS, Xiang R-Z, Chang C-C, Fann W-S. Applied Physics Letters 2004; 84: 1222-1224.

[22] Li D, Wang Y, Xia Y. Advanced Materials (Weinheim, Germany) 2004; 16: 361-366.

[23] Li D, Wang Y, Xia Y. Nano Letters 2003; 3: 1167-1171.

[24] Kit KM, Jagannathan S. Int Nonwoven Tech Conf 2003: 457-467.

[25] Kameoka J, Craighead HG. Applied Physics Letters 2003; 83: 371-373.

[26] Kameoka J, Orth R, Yang YN, Czaplewski D, Mathers R, Coates GW, Craighead HG. Nanotechnology 2003; 14: 1124-1129.

[27] Fennessey SF, Farris RJ. Polymer 2004; 45: 4217-4225.

[28] Deitzel JM, Kleinmeyer JD, Hirvonen JK, Tan NCB. Polymer 2001; 42: 8163-8170.

[29] Lee KH, Kim HY, La YM, Lee DR, Sung NH. Journal of Polymer Science Part B-Polymer Physics 2002; 40: 2259-2268.

[30] The following polymers, polystyrene (PS), poly(methyl methacrylate) (PMMA), poly(2-vinyl pyridine) (P2VP), poly(4-vinyl pyridine) (P4VP), poly(vinyl pyrrolidone) (PVP) and poly(ethylene oxide) (PEO), were all purchased from Aldrich, whereas poly(*l*-lactic acid) (PLLA) and poly(lactic acid-co-glycolic acid) (PLGA) (75:25 lactic:glycolic acid) were generous gifts from Boehringer-Ingelheim Chemicals (Petersburg, VA) and Alkermes (Cincinnati, OH), respectively. Solvents were obtained from Aldrich Chemicals, as was lithium bromide (LiBr). Copper flakes (UCF 8) used in the fiber alignment experiments were available from other studies and is produced by Umicore (Alberta, Canada). All materials were used as received with no further purification.

[31] Kenawy ER, Layman JM, Watkins JR, Bowlin GL, Matthews JA, Simpson DG, Wnek GE. Biomaterials 2003; 24: 907-913.

[32] Shenoy SL, Bates WD, Frisch HL, Wnek GE. Polymer 2005; 46: 3372-3384.

[33] Theron SA, Zussman E, Yarin AL. Polymer 2004; 45: 2017-2030.

[34] Jun Z, Hou HQ, Schaper A, Wendorff JH, Greiner A. E-Polymers 2003: No. 009.

[35] Boland ED, Simpson DG, Wnek GE, Bowlin GL. Polymer Preprints (American Chemical Society, Division of Polymer Chemistry) 2003; 44: 92-93.

[36] Boland ED, Telemeco TA, Simpson DG, Wnek GE, Bowlin GL. Journal of Biomedical Materials Research, Part B: Applied Biomaterials 2004; 71B: 144-152.

[37] Boland ED, Wnek GE, Bowlin GL. Encyclopedia of Biomaterials and Biomedical Engineering 2004; 2: 1246-1253.

[38] Kenawy E-R, Bowlin GL, Mansfield K, Layman J, Simpson DG, Sanders EH, Wnek GE. Journal of Controlled Release 2002; 81: 57-64.

[39] Iba H, Naganuma T, Matsumura K, Kagawa Y. Journal of Materials Science 1999; 34: 5701-5705.

[40] Iba H, Kagawa Y. Philosophical Magazine B: Physics of Condensed Matter: Statistical Mechanics, Electronic, Optical and Magnetic Properties 1998; 78: 37-52.

[41] Iba H, Chang T, Kagawa Y. Composites Science and Technology 2002; 62: 2043-2052.

[42] Naganuma T, Kagawa Y. Acta Materialia 1999; 47: 4321-4327.

[43] Hohman MM, Shin M, Rutledge G, Brenner MP. Physics of Fluids 2001; 13: 2201-2220.

[44] Hohman MM, Shin M, Rutledge G, Brenner MP. Physics of Fluids 2001; 13: 2221-2236.

[45] Lide DR. Handbook of Organic Solvents Boca Raton: CRC Press Inc., 1995.

Table 1. Summary of the polymer/solvent systems investigated for fiber alignment in electrospun mats.

System Polymer / Solvent / Other	M_w ($\times 10^3$) g/mol	[35] wt%	Applied Voltage [d] kV	Fiber	
				Alignment	Diameter [g]
PS / DCM	190	27	17	Yes	
PS / THF	190	30-35	10-20	Yes	10
PS / THF / LiBr [a]	190	20-30	7-17	No	
PS / DMF	190	30	10	No	10
PS / THF / Cu flakes [b]	190	30	17	Yes	
PS / THF	280	22-24	10	Yes	
PMMA / THF	350	14	10-20	Yes	9
P2VP / EtOH	200 [c]	25	14	No	
P2VP / EtOH	200	25	6	Yes	
P2VP / THF	200	25	6	Yes	
P2VP / DCM	200	20	6	Yes	
P4VP / EtOH	200 [c]	25	14	No	
P4VP / EtOH	200	25	6	Yes	
P4VP / DCM	200	20	6	Yes	
PVP / EtOH	1300	10	4	Yes	
PLLA / DCM	670	4.2	20	No [f]	
PLLA / DCM	670	4.2	7	Yes	
PLGA / DCM	300	20	20	No [f]	5 [h]
PLGA / DCM	300	20	7	Yes	6
PEO / H_2O	2000 [c]	3	10-20 [e]	Yes	

[a] Amount of LiBr is 0.20 wt%.
[b] Average Cu flake particle size is ~8 μm.
[c] M_v given not M_w.
[d] Source-to-target distance = 25 cm, unless otherwise indicated.
[e] Source-to-target distance = 15 cm.
[f] Large scale fiber alignment apparent, see text for details.
[g] Average diameter in μm from SEM.
[h] A bimodal distribution of very thin fibers (1 μm) and thicker fibers (10 μm).

Legends for Figures

Figure 1. Schematic diagram of electrospinning instrumentation illustrating chaotic bending instability (A) and stabilized fiber alignment (B).

Figure 2. SEM images demonstrating fiber orientation differences in the absence and presence of LiBr for 30-32 wt% PS/THF solutions electrospun at an applied voltage of 7-10 kV over a 25 cm source-to-target distance: (A) no LiBr (32 wt%, 10 kV) and (B) 0.2 wt% LiBr (30 wt%, 7 kV). Digital photographs for these mats illustrating their effect on light transmission: (C) 130 μm thick PS aligned fiber mat (no LiBr) and (D) 85 μm thick PS non-woven mat (0.2 wt% LiBr).

Figure 3. SEM images demonstrating fiber orientation differences as a function of applied voltage for 20 wt% PLGA/DCM solutions electrospun over a 25 cm source-to-target distance: (A) 7 kV and (B) 20 kV; magnification (×430); (C) 20 kV; magnification (×200); (*note:* the partial alignment at lower magnifications (×200). Transparency effect is shown for the 30 μm thick aligned PLGA mat in (D).

Figure 4. SEM images showing the effect of solvent polarity on fiber alignment in PS electrospun mats from (A) THF and (B) DMF. The polymer concentrations in the two solvents are equivalent and the applied voltage is 10 kV.

Figure 1. Schematic diagram of electrospinning instrumentation illustrating chaotic bending instability (A) and stabilized fiber alignment (B).

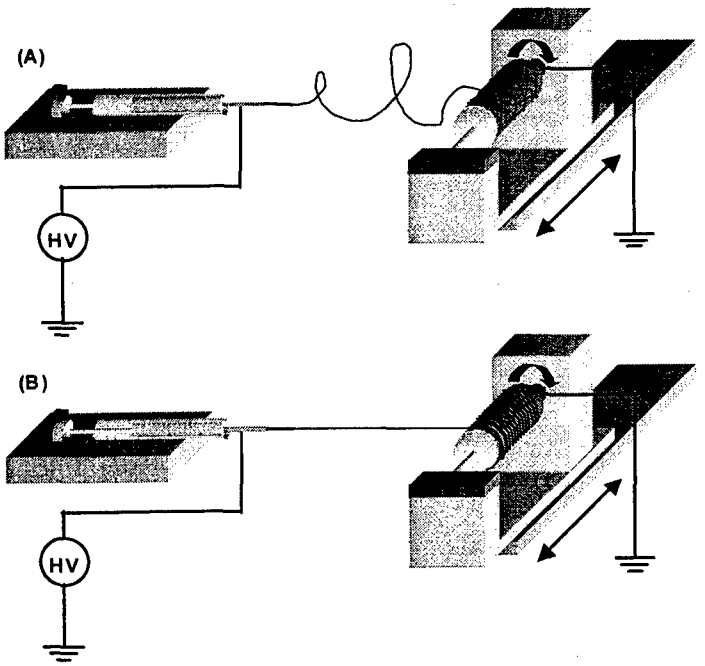

Figure 2. SEM images demonstrating fiber orientation differences in the absence and presence of LiBr for 30-32 wt% PS/THF solutions electrospun at an applied voltage of 7-10 kV over a 25 cm source-to-target distance: (A) no LiBr (32 wt%, 10 kV) and (B) 0.2 wt% LiBr (30 wt%, 7 kV). Digital photographs for these same mats illustrating their effect on light transmission: (C) 130 μm thick PS aligned fiber mat (no LiBr) and (D) 85 μm thick PS non-woven mat (0.2 wt% LiBr).

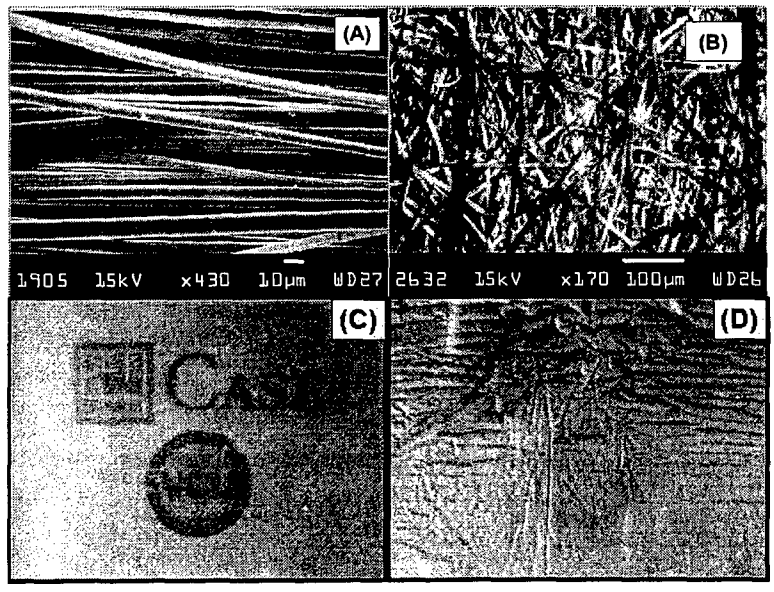

Figure 3. SEM images demonstrating fiber orientation differences as a function of applied voltage for 20 wt% PLGA/DCM solutions electrospun over a 25 cm source-to-target distance: (A) 7 kV and (B) 20 kV (*note:* the observed random fibers at this higher magnification (×430) appear to be aligned at lower magnifications (×100). Transparency effect is shown for the 30 μm thick aligned PLGA mat in (C).

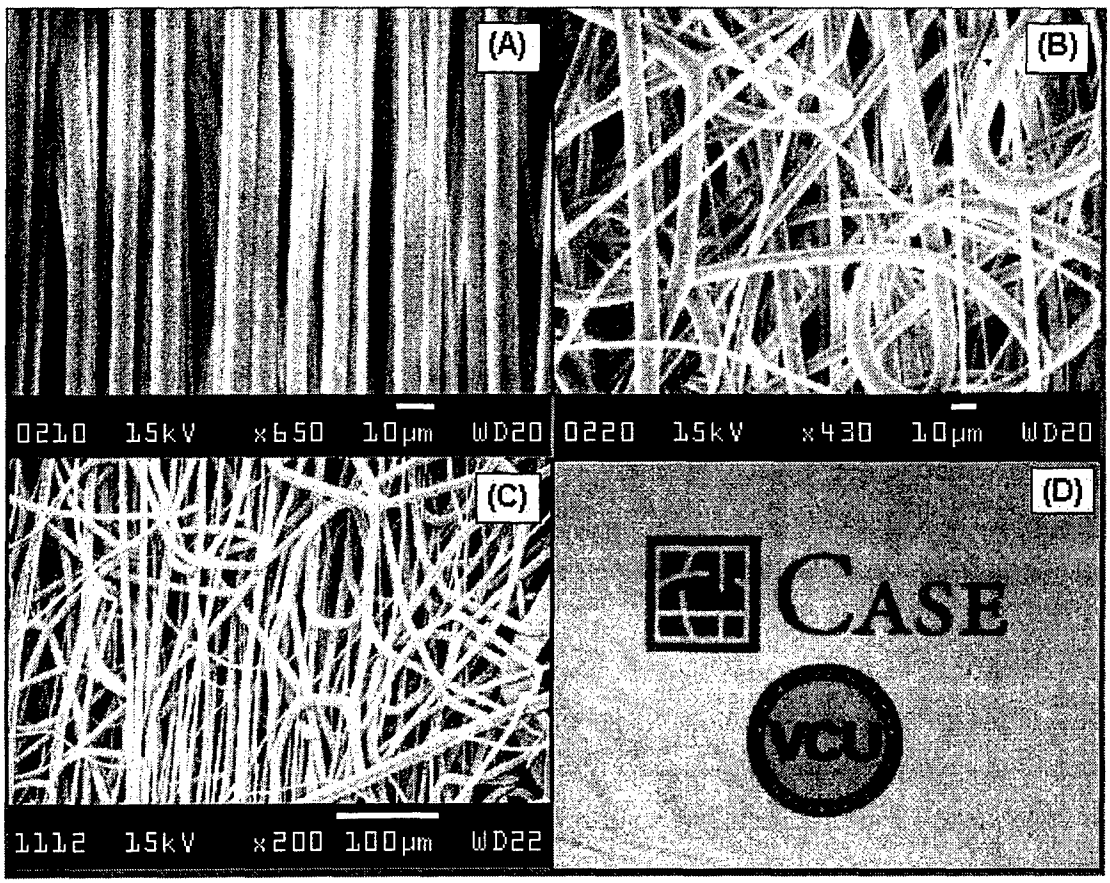

Figure 4. SEM images showing the effect of solvent polarity on fiber alignment in PS electrospun mats from (A) THF and (B) DMF. The polymer concentrations in the two solvents are equivalent and the applied voltage is 10 kV.